

NASA
CR
102240
c. 1

500-TSS-70

RL-SSJ-039

Interim Report ATM Optical Contamination Study

REACTION CONTROL SYSTEM ROCKET ENGINE SPACE PLUME FLOW FIELDS

by B. A. Sodek
C. Y. Chou

LOAN COPY RETURN TO
ARW, TECHNICAL LIBRARY
KIRTLAND AFB, TX

0062632



FACILITY FORM 004	N 69-37277	(ACCESSION NUMBER)
	64	(PAGES)
	CR# 1-234	(NADA CR OR TRX OR AD NUMBER)
	28	(CATEGORY)

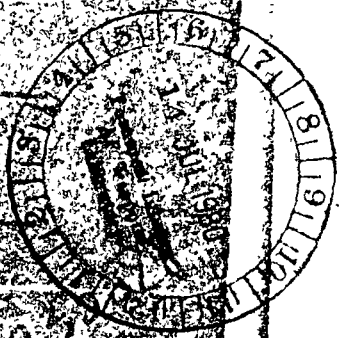


RESEARCH LABORATORIES



BROWN ENGINEERING A TELEDYNE COMPANY

Research Park, Huntsville, Alabama 35894





CR-100,040
INTERIM REPORT
RL-SS1-039

ATM OPTICAL CONTAMINATION STUDY

REACTION CONTROL SYSTEM ROCKET ENGINE SPACE
PLUME FLOW FIELDS

By

B. A. Sodek, Ph.D.
C. Y. Chou

April 1968

Prepared For

PHYSICS AND ASTROPHYSICS DIVISION
SPACE SCIENCES LABORATORY
GEORGE C. MARSHALL SPACE FLIGHT CENTER


Prepared By

RESEARCH LABORATORIES
ADVANCED SYSTEMS AND TECHNOLOGIES
BROWN ENGINEERING COMPANY, INC.
HUNTSVILLE, ALABAMA

ABSTRACT

Apollo Telescope Mount (ATM) experiments are threatened by the scattering, absorption, and deposition effects caused by a cloud of particles ejected from the ATM space complex. This report considers the necessary descriptions of such a contamination cloud and the contribution of reaction control system thrusters to the debris cloud.

Approved:



J. E. White, Jr.
Assistant for Program Management
Advanced Systems and Technologies

TABLE OF CONTENTS

	Page
SUMMARY	1
INTRODUCTION	2
SPACE PLUME FLOW FIELDS FOR RCS ENGINES	4
LM-RCS Plume Flow Fields	10
Discussion of Space Plume Effects	18
APPROXIMATE METHODS OF SPACE PLUME PREDICTIONS	22
The Latvala Approximation	22
The Circular-arc Approximation	27
The Pseudo-nozzle Approximation	30
Comments	33
PARTICLE FIELD INTERACTIONS	34
Dwell-time and Particle Distribution	34
Optical Interference by Debris Cloud	39
Future Plans	40
APPENDIX A. ANALYSIS OF AN IDEAL ROCKET	41
APPENDIX B. REACTION CONTROL SYSTEM ENGINE CHARACTERISTICS	48
APPENDIX C. RCS PARTICLE LIFETIME	52
REFERENCES	53

LIST OF ILLUSTRATIONS

Figure		Page
1	General Description of Exhaust Jet (From Ref. 17) . . .	5
2	Prandtl-Meyer Turning Angles as a Function of Nozzle Exit Mach Number	8
3	Service Module RCS Space Plume, $\epsilon = 40$ (From Ref. 1)	9
4	General Configuration, LM/ATM (From Ref. 2) . . .	11
5	LM-RCS Nozzle Contour (From Ref. 2)	12
6	Real-gas and Ideal-gas Mach Contours for LM-RCS Thrusters (From Ref. 4)	13
7	Present Stored Configuration (From Ref. 2)	16
8	Present Deployed Configuration (From Ref. 2) . . .	17
9	Deflector on Present Configuration (From Ref. 2) . .	19
10	Jet Radial Flow and Geometry Definition (From Ref. 10)	23
11	Radius Ratio of Jet Boundary for $\gamma = 1.4$ (From Ref. 10)	28
12	Circular-arc Approximation Compared with Method- of-characteristics Solution (From Ref. 10)	29
13	Particle Source Region	36
14	Parameters for Description of Particles in Debris Cloud	38
A-1	Simple Rocket Thrust Chamber (From Ref. 10) . . .	42
A-2	Spherically Symmetric Nozzle Flow (From Ref. 20) .	46
B-1	RCS Nozzles (From Ref. 1)	51

LIST OF SYMBOLS

A	Area
a	Speed of sound
C_d	Discharge coefficient
C_F	Thrust coefficient
c^*	Characteristic velocity
c_p	Specific heat at constant pressure
D	Diameter
F	Field of view
f	Force
g	Acceleration of gravity
h	Enthalpy
L	Length
M	Mach number
\bar{M}	Mean molecular weight
\dot{m}	Mass flow per unit time
n	Particle number density
p	Pressure
Q_R	Quantity of heat
r, R	Radial coordinate
R_M	Characteristic radius of debris cloud

LIST OF SYMBOLS - Continued

R_s	Radius of space vehicle
s	Entropy
T	Temperature
t	Time
u	Velocity, x-component of velocity
u_0	Initial ejection velocity
\dot{u}	Acceleration
v, V	Velocity, y-component of velocity
w	z-component of velocity
x, X	Linear coordinate
y	Rectangular coordinate
z	Rectangular coordinate
α	Plume boundary angle
γ	Ratio of specific heats
δ	Small positive exponent
ϵ	Area expansion ratio
θ_c	Contraction half angle
θ_N	Nozzle half angle
ν	Prandtl-Meyer expansion angle
ρ	Density
σ	Nondimensional radial coordinate
Γ	Thrust

LIST OF SYMBOLS - Concluded

τ	Lifetime
ϕ	Azimuthal angle with respect to nozzle axis
Ω	Solid angle

Subscripts

a	Ambient
B	Boundary
c	Chamber
e	Exit plane
m	Point of maximum plume diameter
n	Point on plume boundary
t	Throat
T	Total
o	Stagnation state

LIST OF ABBREVIATIONS

AEDC	Arnold Engineering Development Center
ATM	Apollo Telescope Mount
BBRC	Ball Brothers Research Corporation
CM	Command Module
ECS	Environmental Control System
LM	Lunar Module
MMH	Monomethylhydrazine
RCS	Reaction Control System
SM	Service Module
UDMH	Unsymmetrical dimethylhydrazine
WMS	Waste Management System
50/50	Fuel mixture of 50-percent UDMH and 50-percent hydrazine

SUMMARY

The description of high-altitude rocket exhaust plumes is discussed. Method-of-characteristics solutions for the Service Module-reaction control system (PCS) and the Lunar Module-RCS space plumes are presented. An indication of shock waves formed by the LM/ATM structure and its solar panels is also presented. The major threats of RCS contamination are the contribution to a debris cloud and the deposition of material onto critical surfaces. No direct impingement effects seem indicated, but the interference of an boundary layer formed by the LM/ATM structure provide mechanisms for possible contamination particles to reach the interior of the ATM experiment rack. Deposition on sensitive elements may be simulated by test rocket firings, but more reliable criteria will be developed by space flight experiments. Available study of the possibility of contamination indicates the advisability of using a cover for the experiment tube.

Approximate methods of plume description, the Latvala method, the circular-arc method, and the pseudo-nozzle scheme are described for possible future use. A general description of particles emanating from the spacecraft, especially gaseous leaks, should be similar to the approximate method discussed.

An assumption of spherical symmetry of debris cloud is not justified. The impossibility of describing individual particle trajectories and resulting cloud absorption and extinction leads to plans for the calculation of Rayleigh and Mie scattering and an estimate of the large particle effects.

INTRODUCTION

Apollo Telescope Mount (ATM) experiments are threatened by contamination particles emanating from the space vehicle cluster. One of the principal sources of such material is the reaction control system attitude control thrusters. Exhaust products not only provide material for the formation of a debris cloud but also for deposition onto sensitive elements of the experimental package and spacecraft sensors.

The possibility of contamination of ATM experiments by reaction control system exhaust gases may be examined on the basis of two factors

- o The amount of the material contributed to the debris cloud
- o The amount of such material deposited on functional surfaces.

These factors will be analyzed through the use of the known geometry of space plumes produced by specific ATM and cluster rocket engines and time sequences of ATM activities. The space plumes of SM- and LM-RCS engines are discussed in this report.

The exhaust jet plume at high altitudes is discussed and described. Results of specific calculations for SM-RCS and LM-RCS space plume flow fields are also presented. A discussion of mechanisms for the transfer of exhausted material into the vicinity of the ATM tube indicates the need for an aperture cover, controllable by the crew, for the experiment tube. Approximate methods of making further calculations of plume boundaries and flow fields are discussed. Previous assumptions of spherical symmetry in the debris cloud are found to be unacceptable. The general theoretical approach (which, unfortunately, is impractical) can be approached by describing the effects of a debris cloud in terms of reasonable ranges of cloud parameters. These considerations are discussed. Future plans are also discussed in this section. There are

four appendices in this report. The theory of the ideal rocket is presented in Appendix A. This provides a basis of comparison with more sophisticated approaches and some isentropic flow-field descriptions for use with the approximation given in this report. Collected characteristics and nozzle geometries are presented in Appendix B. A correction of previous estimates of RCS particle lifetime in the vicinity of the ATM is found in Appendix C.

SPACE PLUME FLOW FIELDS FOR RCS ENGINES

The structure of the exhaust plume produced by rocket engines, ejecting into a highly rarefied atmosphere, is basically as illustrated in Figure 1. The more important features of a typical exhaust plume consist of the leading characteristic line, internal shock, jet boundary, and normal shock. The normal shock is also referred to as a Riemann-wave or Mach disk.

The leading characteristic or Mach line, as determined from the nozzle exit Mach number, is a straight line for the contoured nozzle and forms the familiar Mach cone. All flow conditions along this Mach line and within the Mach cone are one-dimensional for the simplest case. For the conical nozzle, the leading characteristic line is curved; and the flow within the curved cone is radial and axisymmetric. For both nozzles, operating above the design pressure ratio, the leading characteristic serves as a dividing line between two different flow regions. The internal region consists of a zone of zero external influence in which flow properties are determined strictly from nozzle properties. The flow characteristics of the region external to this line and bordered by the jet boundary are controlled by the ratio of stagnation pressure to ambient pressure.

The isentropic expansion process in the region bounded by the leading characteristic line, the axial center line, the normal shock, and the internal shock is initiated by the corner expansion fan, originating at the nozzle lip. Mach numbers within this region increase continuously both with distance downstream of the nozzle exit and also in a direction perpendicular to the axis out to the position of the internal shock. In addition, the internal shock, which is formed by the coalescence of infinitesimally weak compression waves reflected from the jet boundary, starts near the nozzle lip and increases in strength in the downstream

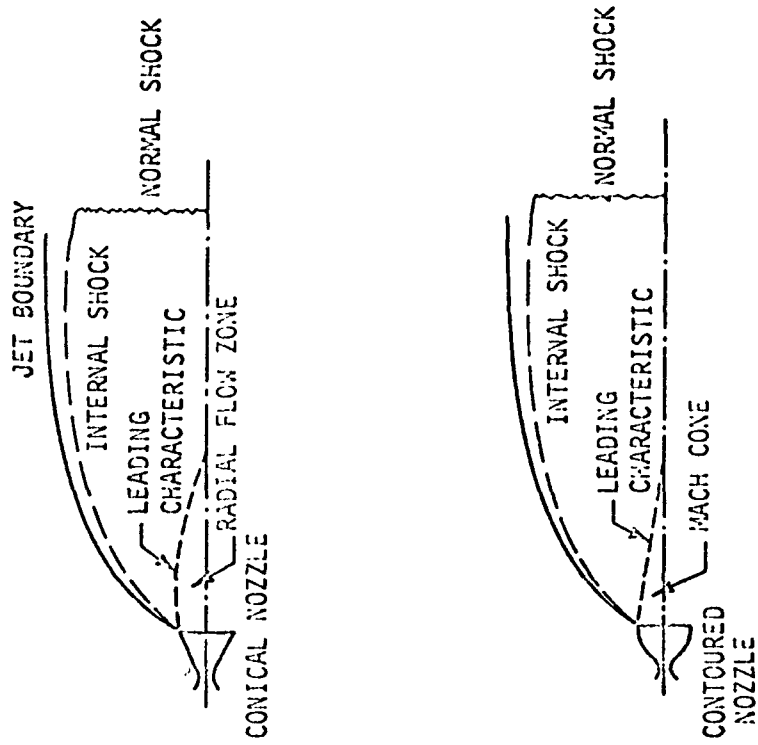


FIGURE 1. GENERAL DESCRIPTION OF EXHAUST JET (FROM REF. 17)

direction. For large pressure ratios, the internal shock system forms the familiar shock diamond pattern. As the ratio of stagnation to ambient pressure increases greatly in the orbital environment, a normal shock replaces the intersection of the X-type shocks; and the internal shock approaches the jet boundary. The jet boundary defines the external shape of the exhaust plume and is the separation line between ambient conditions and flow from the exhaust nozzle.

To simplify calculation procedures, equilibrium in the plume is assumed. The angle through which the flow turns at the nozzle lip corresponds to a Prandtl-Meyer expansion from the nozzle exit Mach number to the boundary Mach number. The boundary Mach number depends on the ambient pressure at any particular altitude. The flow direction, after the expansion, is determined by adding the slope of the nozzle wall at the exit to the amount of Prandtl-Meyer (P-M) turn. The boundary angle α that the tangent to the plume at the nozzle lip makes with the axis of the nozzle is the sum of three component angles

$$\alpha = \nu_1 - \nu + \theta_N \quad (1)$$

where

- α - net boundary angle sought
- ν_1 - maximum expansion angle given by the P-M equation for expansion from $M = 1$ at the throat to M_B at the boundary or ambient pressure
- ν - expansion angle from the P-M equation for expansion from $M = 1$ to M_c at the nozzle lip
- θ_N - nozzle half angle.

The equation for the P-M wave expansion angle is the integral of the differential equation

$$d\nu = \left(M^2 - 1 \right)^{\frac{1}{2}} \left(\frac{dV}{V} \right) \quad (2)$$

which is the basis of the method-of-characteristics solution. The integration of Equation 2 is

$$v = \left(\frac{\gamma + 1}{\gamma - 1}\right)^{\frac{1}{2}} \tan^{-1} \cdot \left(\frac{\gamma - 1}{\gamma + 1}\right)^{\frac{1}{2}} \left(M^2 - 1\right)^{\frac{1}{2}} - \tan^{-1} \left(M^2 - 1\right)^{\frac{1}{2}} \quad (3)$$

A graph of turning angle as a function of exit Mach number for a γ of 1.25 is shown in Figure 2.

Before a prediction can be made of the effects of an impinging plume on a surface or material complex, the external exhaust flow field must be established. In addition to the jet boundary angle, thermodynamic properties and the flow field at the nozzle exit plane must be known. The conditions at the nozzle exit plane may be found from manufacturer's engine-performance data and theoretical one-dimensional performance calculations. Such a scheme assumes one-dimensional nozzle flow with shifting equilibrium to the throat and frozen flow thereafter. The specific impulse ratio of specific heats, pressure ratio, and temperature are obtained from manufacturer's specifications, if possible, for the engine operating at a normal mixture ratio.

An analysis of an ideal rocket is presented in Appendix A. Specific characteristics of the RCS engines of primary concern are given in Appendix B. The isentropic formulas and manufacturer's specifications discussed in these appendices provide information equivalent to the input data of a method-of-characteristic program which would usually be restricted to constant exit plane properties. A space exhaust flow field calculated for an SM-RCS engine is presented in Figure 3. The space boundary in the illustration was calculated by means of the P-M expansion. The term X is a coordinate along the axis; R is a coordinate radial to the axis; R_c is the nozzle exit ratio; and ϵ is the nozzle expansion ratio. The curves of constant Mach number within the plume may also be considered to be contours of constant density or temperature if flow is assumed to be isentropic.

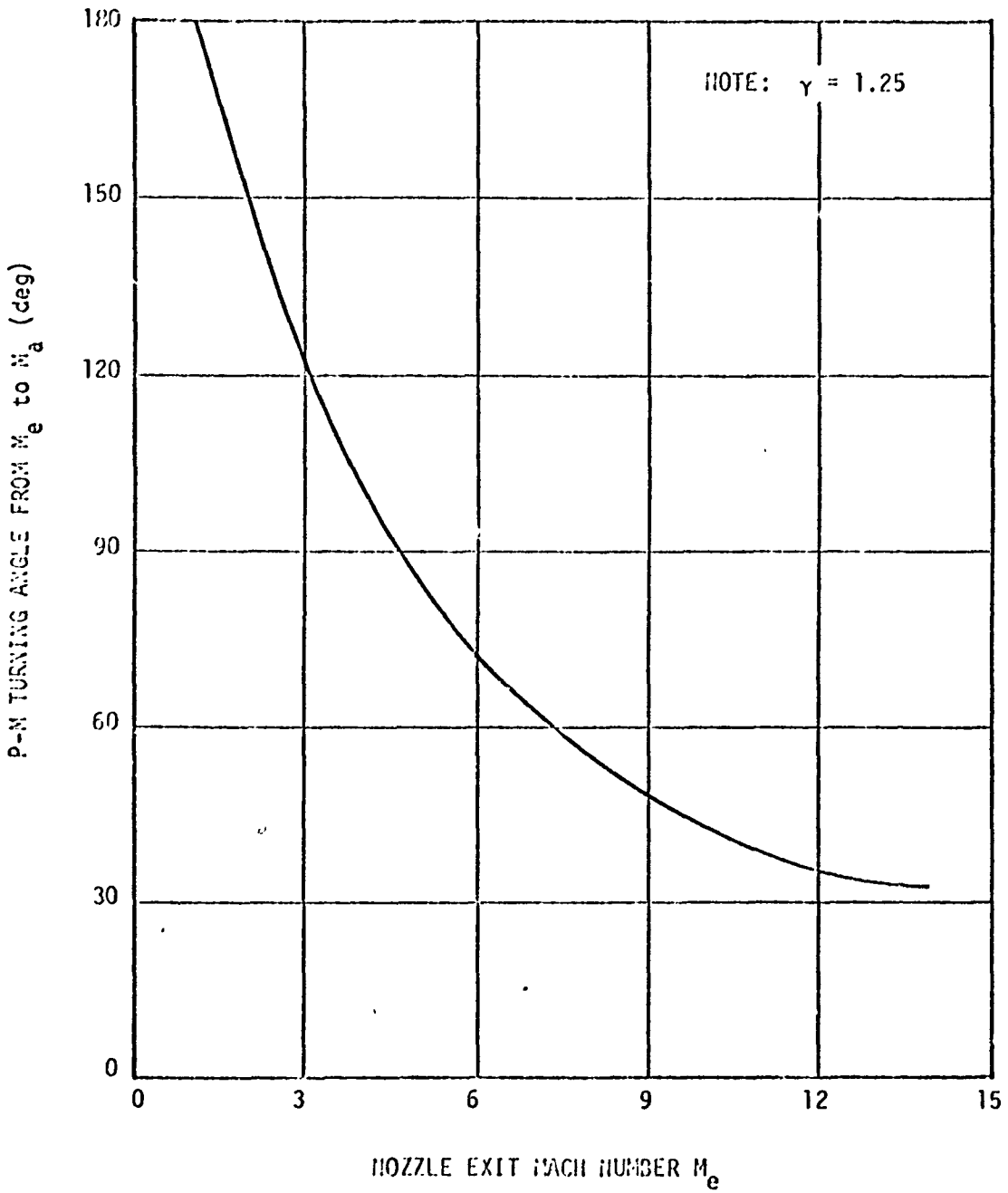


FIGURE 2. PRANDTL-MEYER TURNING ANGLES AS A FUNCTION OF NOZZLE EXIT MACH NUMBER

REPRODUCIBILITY OF THE ORIGINAL PAGE IS POOR

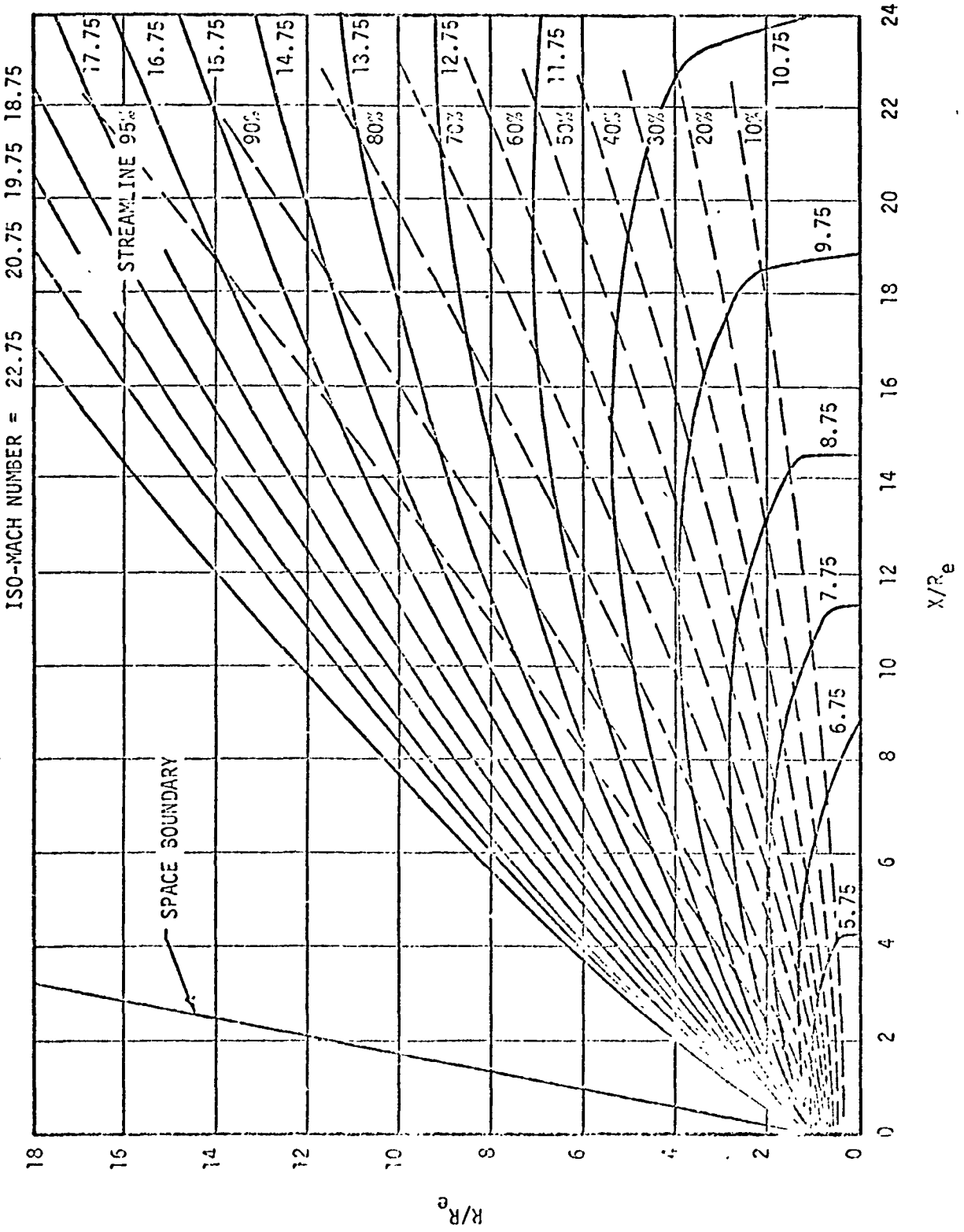


FIGURE 3. SERVICE MODULE RCS SPACE PLUME, $\epsilon = 40$ (FROM REF. 1)

LM-RCS PLUME FLOW FIELDS

A more realistic description of the space plume due to an RCS engine thruster, in this case the SM-RCS or LM/ATM-RCS engine, has been generated because of the necessity of examining the structural and performance integrity of the solar panels attached to the ATM rack.

To avoid heating and thrust degradation, Loeb (Ref. 2) has recommended the use of a small deflector shield for those RCS thrusters whose plume impinges upon the ATM solar panels. Whether such an addition has been made is not known. The presently proposed configuration of the LM and the ATM experiment rack are shown in Figure 4. The unfortunate positioning of the LM Service Module RCS is a result of prior design requirements of docking capability and solar panel deployment spacing. The thrusters in the minus X direction will produce plumes which impinge directly upon the rack solar panels in both their stored and deployed positions. This plume impingement creates a severe heating environment for both the solar panels and the instruments on the rack structure. In addition, much actual thrust is lost because of this mass impingement on the panels. The interference of exhaust plumes with the structure of the LM/ATM and rack will produce a system of standing shocks near various surfaces. It is expected that boundary layers will form over all impinged surfaces providing a mechanism for mass flow in to the rack interior.

A real-gas equilibrium analysis was used to calculate the flow properties of the exhaust plume as produced by the LM-RCS rocket engine. This engine burns 50/50 and N_2O_4 . The nozzle contour is shown in Figure 5. This plume is slightly more severe (lower Mach numbers at greater distances from the exit plane) than the perfect gas solutions (Ref. 3 and 4); it is represented in Figure 6, which shows the Mach number contours of the LM-RCS plume.

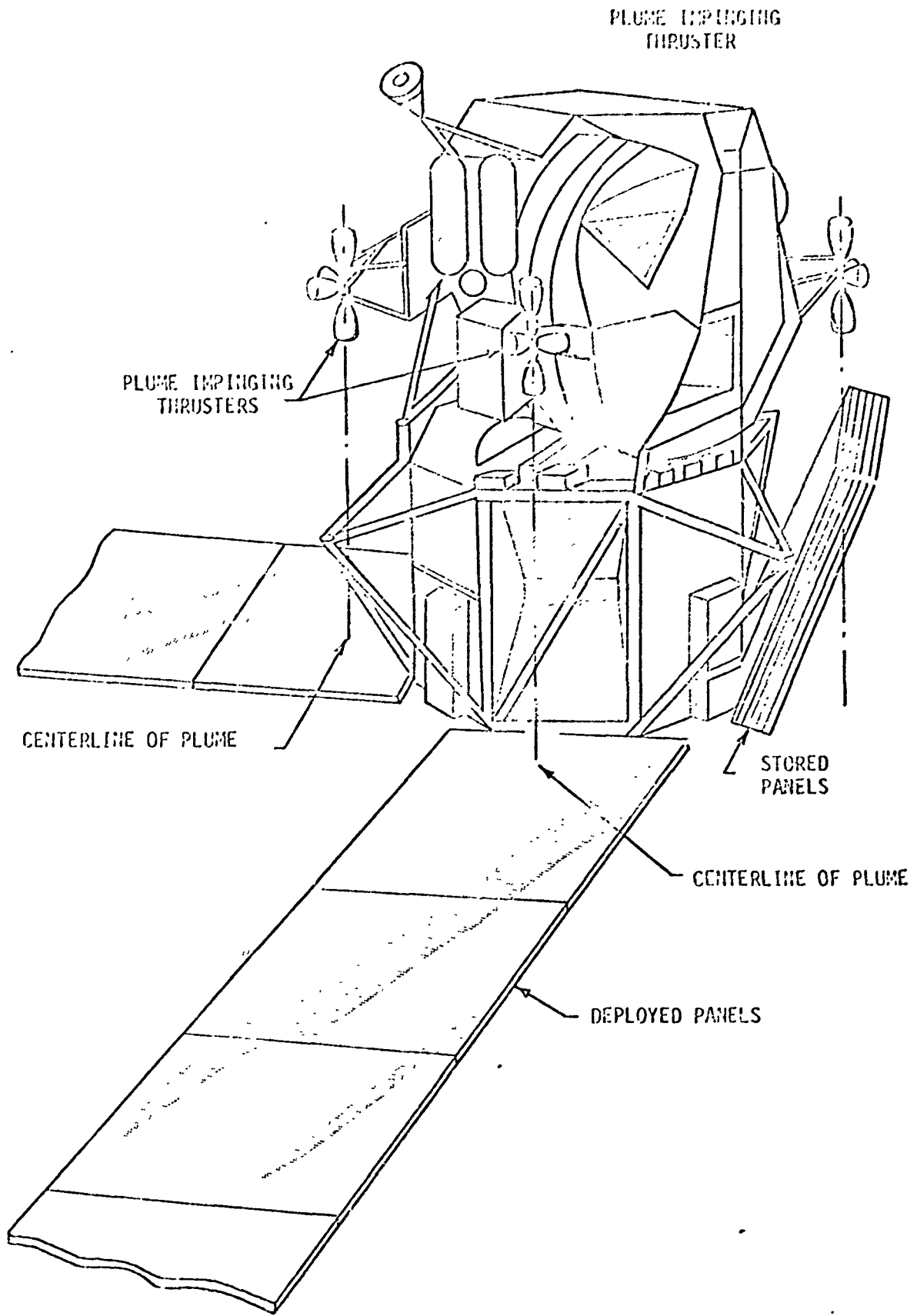
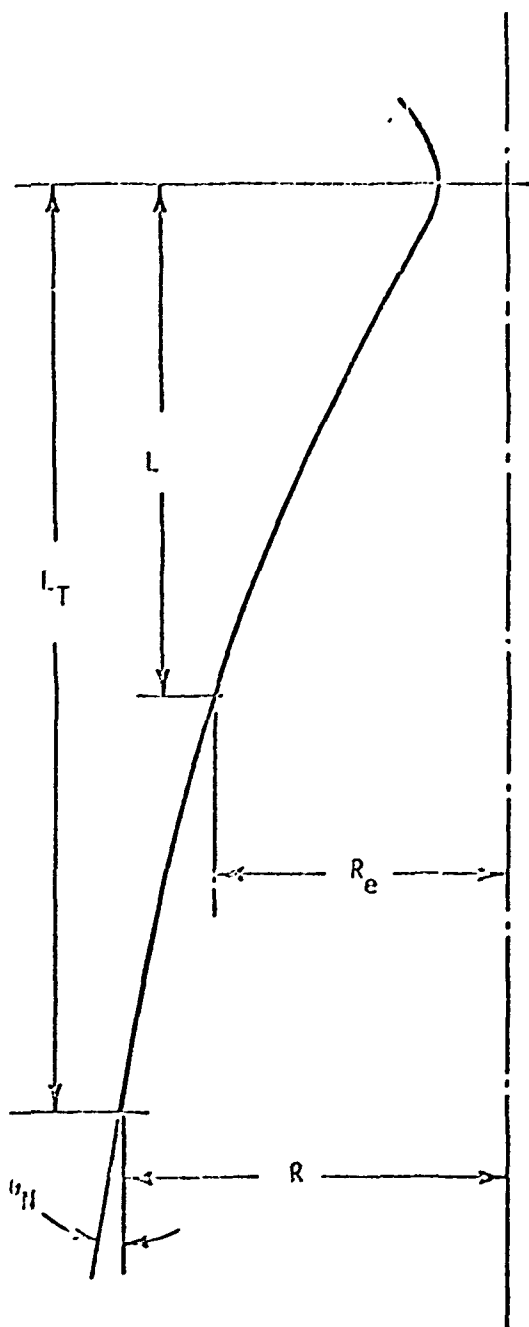


FIGURE 4. GENERAL CONFIGURATION, LM/ATM (FROM REF. 2)



NOZZLE DIMENSIONS	
ϵ	40.0 in
R_e	2.730 in.
L_T	6.984 in.
θ_H	8.3°

NOZZLE COORDINATES	
L (in.)	R (in.)
0.000	0.434
0.278	0.513
0.474	0.635
0.812	0.832
1.339	1.106
1.866	1.349
2.393	1.565
2.920	1.762
3.447	1.939
3.974	2.101
4.501	2.245
5.028	2.372
5.555	2.483
6.082	2.583
6.609	2.671
6.984	2.730

FIGURE 5. LH-RCS NOZZLE CONTOUR (FROM REF. 2)

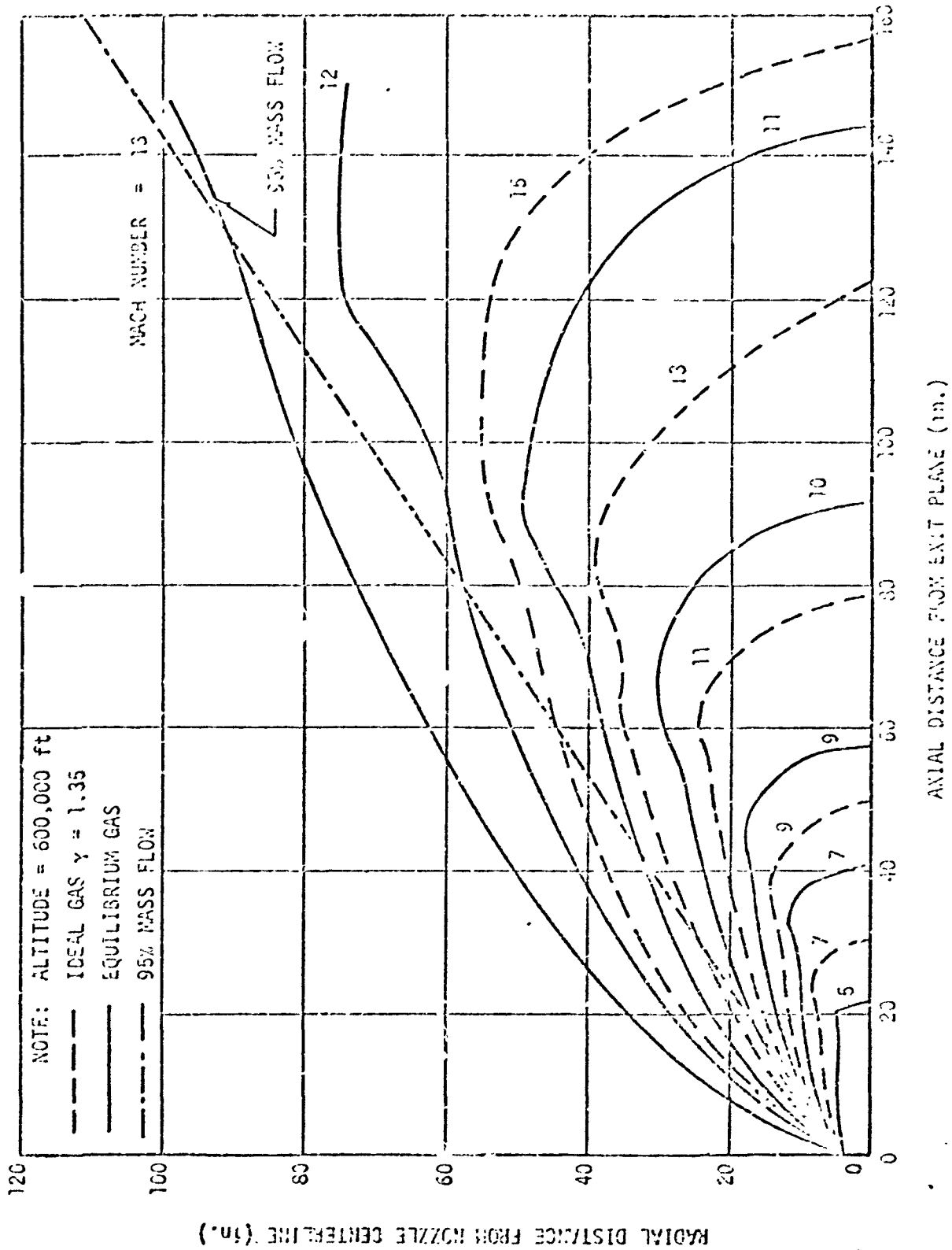


FIGURE 6. REAL-GAS AND IDEAL-GAS MACH CONTOURS FOR LM-103 THRUSTERS (FROM REF. 4)

Calculations for the LM-RCS nozzle equilibrium flow field using the nozzle contour (Ref. 2) were made for an equilibrium reacting gas. A second flow field was also generated for an ideal gas. Both flow fields were obtained using the method-of-characteristics program described in Reference 5. The flow fields are compared by considering the parameters associated with the same geometrical location in each field. In general, the plume for the ideal-gas assumption gives higher Mach numbers for a given axial and radial position.

The discrepancy between the real-gas and ideal-gas flow fields results from basic differences in theory for the two problems. For the ideal-gas assumption, the molecular weight does not change. The specific heats are assumed to be constant, and enthalpy is a function of temperature only. These assumptions result in a greatly simplified system of equations, describing the plume flow field.

For the equilibrium-reacting gas case, the conservation of the various species of gaseous components must be considered as well as the chemical kinetics of the problem. The molecular weight and isentropic exponent of the mixture are not constant in the plume, thus complicating the equations describing the flow field. In general, the flow parameters are no longer simple functions of temperature or velocity but depend on the local velocity and entropy. These complications affect the method-of-characteristic solution and the shock relations and result in values of the flow-field parameters which are different from those generated using ideal-gas theory. Specific differences in an ideal-gas solution and an equilibrium-reacting gas solution would depend on the gas properties specified in each case.

The LM-RCS thruster exhaust gases are actually composed of a reacting-gas mixture in which the molecular weight and isentropic exponent are not constant. The use of the ideal-gas assumption would

result in a rough approximation of the flow fields at best. Since the gas mixture can be considered to be in local equilibrium at any instant, the plume flow field is calculated by the real-gas method. The most important real-gas effect on the plume is the reduction of the Mach number of the gases at any point in the near plume. This reduction in Mach number results in the predicted impingement heating rates being conservative. The heating rates are predicted based on ideal-gas analysis.

The line which contains 95 percent of the mass flow (Figure 6) may be considered to define the "core" of the space plume.

Firing of the LM-RCS thruster may occur while the panels are either stored or deployed. Lockheed (Ref. 6) reports that serious heating and thrust degradation occur with the panel in either position. Figure 7 shows the stored panels and the thruster plume interaction shocks over the panels in this position. The oblique shocks were calculated by the method-of-characteristics program, with a two-dimensional assumption being used to approximate the flow field over the configuration (Ref. 5). These shocks arise from the top of the panels and from the structural members of the rack and will create a hot stagnation region in the interior portion of the rack as well as high heat rates to the top side of the stored panels. Also, the impingement of the rarefied upper portion of the plume onto the upper structure, and gaseous radiation from the plume to this upper structure will create additional heating of the rack structure.

When the solar panels are deployed, a large normal shock forms over the flat expanse of the inner panels (Figure 8). Because of the substantial amount of the mass flow which impinges on the panels, the effective thrust of the LM-RCS engine is nullified.

SCALE: 1 cm \approx 10 in.

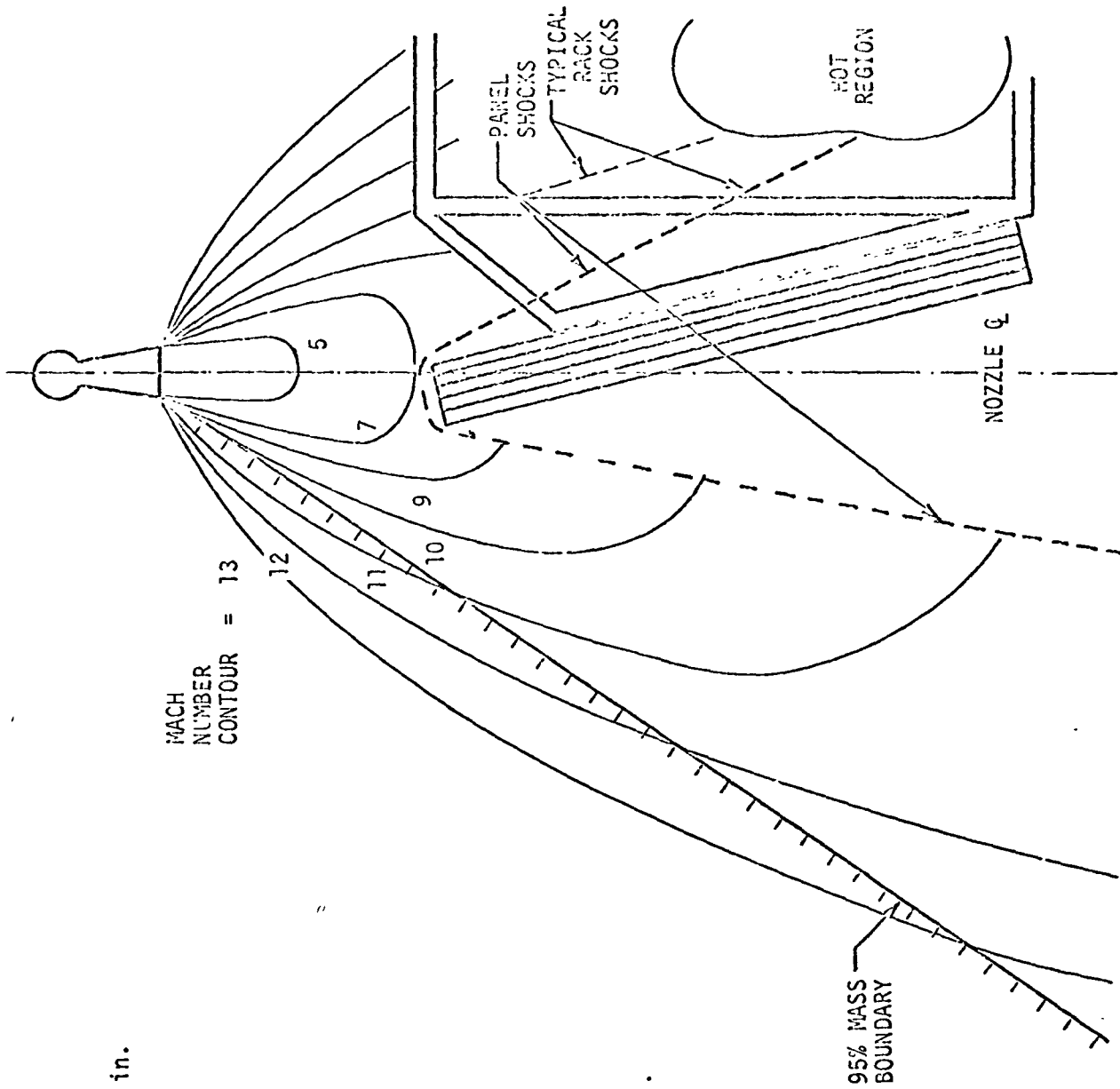


FIGURE 7. PRESENT STORED CONFIGURATION (FROM REF. 2)

SCALE: 1 cm \approx 10 in.

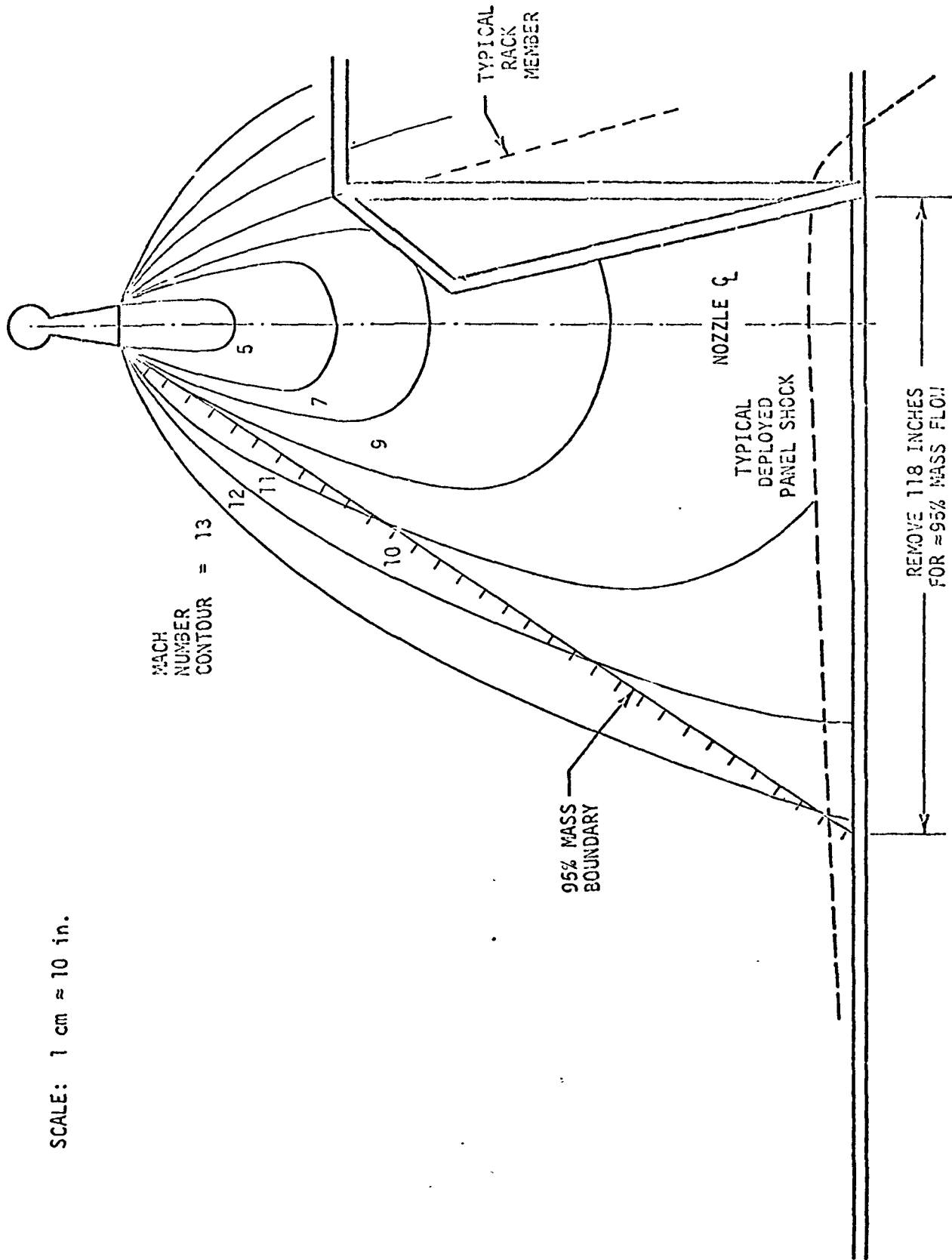


FIGURE 8. PRESENT DEPLOYED CONFIGURATION (FROM REF. 2)

If the solar panels are to be deployed during the thrusting operation, a portion of the panels should be removed in the area where 95 percent of the plume impinges on the panels (Ref., 2). The shock arising from the deflector (Figure 9) and the diverted mass flow of the plume aft of the bottom lip of the shield create a plume that is smaller at the plane of the deployed panels than the plumes without deflectors. This would indicate that perhaps still less of the panel area need be removed if a shield shape were optimized for this situation.

This method of deflecting the flow field with an Inconel steel deflector (0.1-inch thick) shows the most promise of the several designs investigated in this study. No major thruster reorientation is necessary, and the capability of the Inconel to withstand the incurred heating rates has been found to be adequate. The scoop-like configuration is shown in Figure 9 along with the results of a two-dimensional analysis of the plume and consequent shock interaction with the shield.

DISCUSSION OF SPACE PLUME EFFECTS

The effects of rocket exhaust gas plumes in the space environment have generally been discussed as direct effects, principally heating of spacecraft elements, thrust degradation due to interfering surfaces, or impulsive damage to structural members produced by impingement. Several analyses have been made concerning the problems, particularly for the Lunar Module and Apollo spacecraft (Refs. 2 and 3). Possible confusion of infrared sensors because of plume radiation has also been considered (Refs. 7 and 8). Some information pertinent to the threat of contamination or of information degradation of ATM experiments has been obtained from such sources. The main purpose of those studies differs, however, from that of the present effort. The important questions which must be answered concerning the degradation and contamination of space science experiments are

SCALE: 1 cm \approx 10 in.

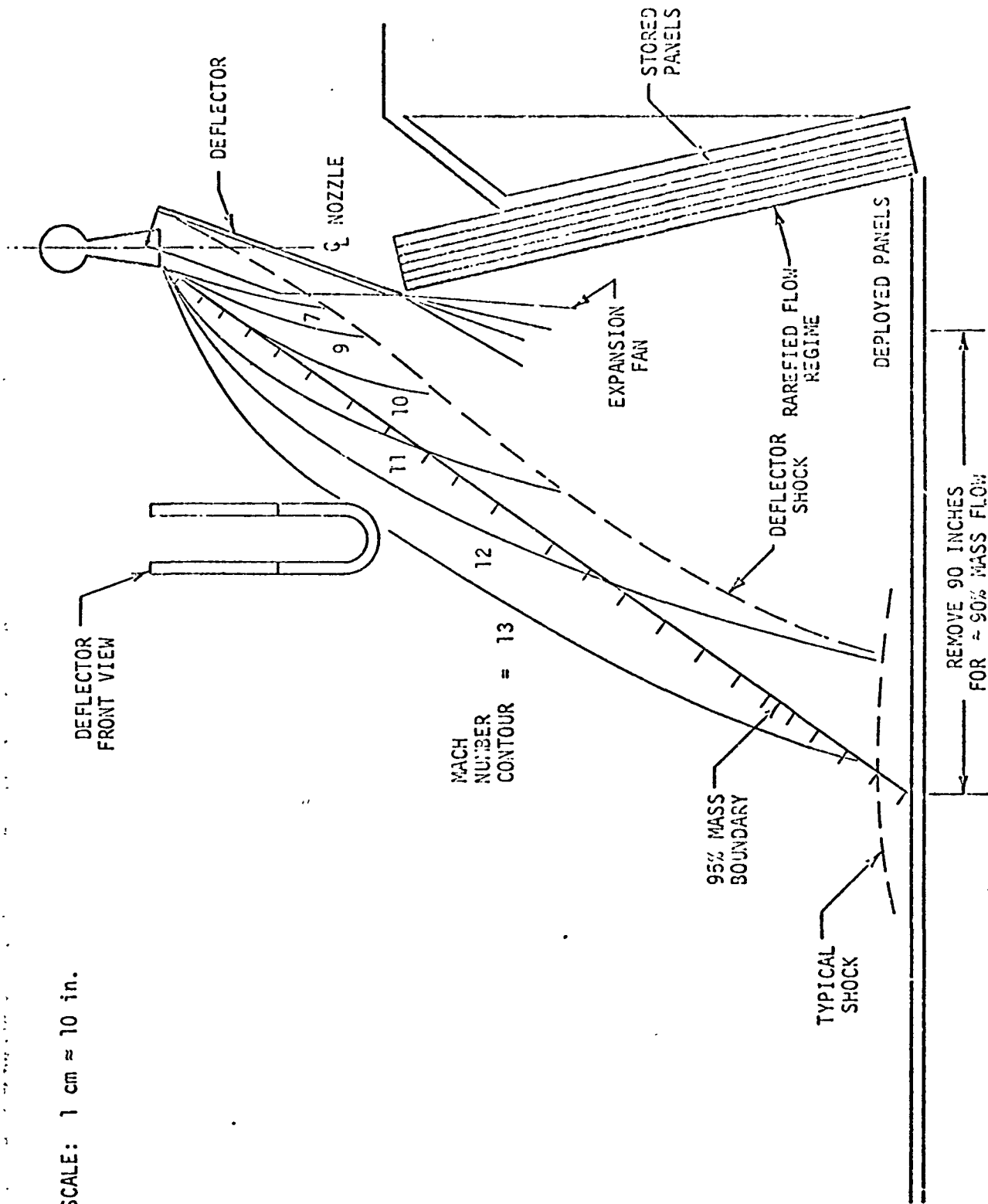


FIGURE 9. DEFLECTOR ON PRESENT CONFIGURATION (FROM REF. 2)

- o How much material is provided for the formation of a debris cloud by rocket firings in the space environment?
- o How much material is deposited onto sensitive areas with significant effects because of rocket firings?

The answers to these questions will be built on the known geometry of space plumes produced by specific ATM and cluster rocket engines and time sequences of planned ATM activities. Event description of and sequencing of steps in rendezvous, docking, observing, orbital change, astronaut departure, and station keeping are not yet clearly defined. Each of these phases could involve extraordinary rocket firing. The ATM experiment package should be protected during these activities.

The contribution of RCS exhaust products will be more fully discussed when propellant consumption and debris cloud behavior are better understood. Some estimates of "worst case" cloud absorptions were presented in Reference 8. The deposition of matter from the plume, interaction of reducing chemicals in the plume with sensitive functional surfaces, and the presence of large ($\geq 100 \mu$) particles in the flow field (from fuel contaminants, engine erosion products, or charred bits resulting from ablation cooling) may significantly harm components such as optical transmission elements, solar cell panels, and thermal control coatings.

The expanding plume strikes the exterior of the ATM experiment rack, but no direct impingement of rocket exhaust gases from the RCS thrusters is expected on the contents of the interior. The space core from certain thrusters passes over the open top of the rack. Drift and turbulence may be expected to move material from the plume into the experiment rack. The formation of a boundary layer and subsequent creep of material along the exterior of the rack is to be expected and is the most likely mechanism for mass flow into the ATM tube.

The interaction of a rocket plume with any surface should produce standing shock waves at some distance from the obstructing surface. This facilitates concentration of material at the shock lines and provides for mass flow over the surface.

The nature of the plume flow field changes when the surface of a space vehicle is encountered. The nature of the change and boundary layer activity cannot be well predicted. A region of turbulence should spread from the first impact area on a vertical wall toward the entrance to the rack. At the lip of the rack, the edge provides another source of disturbance to complicate the flow. Without doubt, mechanisms exist for supplying material to the interior of the tube. Creeping in the boundary layer and streamline deflections at the rack's edge aid mass flow towards the experiment package. Exhaust gas contamination of internal surfaces may also occur when several thrusters are firing. Recirculation of exhaust gases (similar to that in the base region of a launch vehicle) in the region of the rack aperture could cause migration of exhaust products into the interior, where deposits could accumulate.

Laboratory tests may possibly be able to gauge the extent of information degradation by a debris cloud near the observing instruments. Test chamber firings of rockets or scale-model rockets may provide estimates of deposition and the deposition rate as a function of firing time. More suitable measurements of the amount and composition of particles, in addition to gaseous components, due to rocket exhausts will be available from planned space experiments.

In previous investigations (Ref. 9), recommendations were made that an aperture cover be provided for the ATM experiment rack for use during launch, environmental control system and waste management system dumps, and RCS firing. Present investigations also indicate the need for an ATM cover during these and other phases of a particular mission, such as docking, major orbital changes, and astronaut departure. As a general rule, the aperture should be closed whenever the ATM is not being used for observation.

APPROXIMATE METHODS OF SPACE PLUME PREDICTIONS

Extensive calculations are required for the method-of-characteristics program solutions describing space plumes. These yield profiles for only one time and one altitude. It is expected that for rapid consideration of plume boundaries and flow fields approximate methods (simpler in scope and exercise than the method-of-characteristics) should be examined.

A number of approximations have been developed for the prediction of jet exhausts as a function of altitude and nozzle properties. Such schemes almost invariably consider a jet exhausting into a still atmosphere. The most widely used approximation, due to Latvala (Ref. 10), assumes isentropic flow and uses the Equation 1 Prandtl-Meyer turning angle as a starting point.

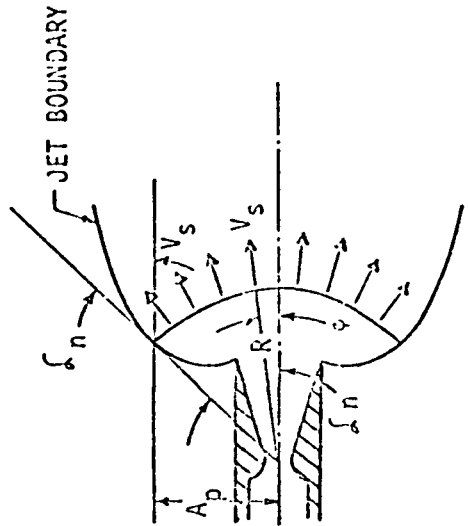
THE LATVALA APPROXIMATION

Latvala presented a very detailed and convenient description of his analytical method for predicting the boundary of jets at high altitude. The sketches in Figure 10 illustrate the geometry involved in his analysis.

When radial, axisymmetric, isentropic flow of a perfect gas is assumed, the equations for continuity and conservation of energy between any two points, n and $n + 1$, may be written for a free jet as

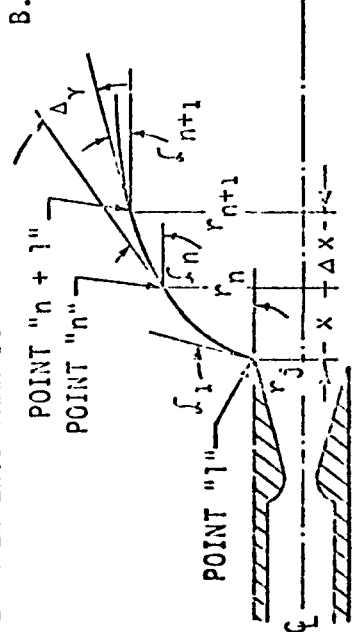
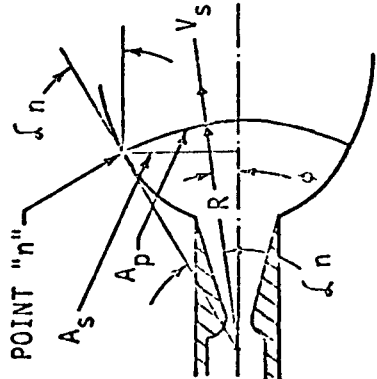
$$\rho_n A_n V_n = \rho_{n+1} A_{n+1} V_{n+1} \quad (4)$$

$$c_p T_n + \frac{V_n^2}{2} = c_p T_{n+1} + \frac{V_{n+1}^2}{2} \quad (5)$$



A. INITIAL ANGLE LESS THAN 90°

B. INITIAL ANGLE GREATER THAN 90°



C. ILLUSTRATION OF POINTS n and n+1

FIGURE 10. JET RADIAL FLOW AND GEOMETRY DEFINITION (FROM REF. 10)

The first equation is solved for V_{n+1} and substituted into the second equation,

$$\frac{A_{n+1}}{A_n} = \frac{\rho_n}{\rho_{n+1}} \left[\frac{2 c_p T_n}{V_n^2} \left(1 - \frac{T_{n+1}}{T_n} \right) + 1 \right]^{-\frac{1}{2}} \quad (6)$$

Since the flow is isentropic,

$$\frac{\rho_t}{\rho} = \left[1 + \frac{1}{2} (\gamma - 1) M^2 \right]^{\frac{1}{\gamma-1}} \quad (7)$$

$$\frac{T_t}{T} = 1 + \frac{1}{2} (\gamma - 1) M^2 \quad (8)$$

Equations 7 and 8 may be combined with Equation 6, with the definitions of the Mach number, to give

$$M^2 = V^2 / \gamma R T \quad (9)$$

and the specific heat at constant pressure

$$c_p = \gamma R / (\gamma - 1) \quad (10)$$

to yield

$$\frac{A_{n+1}}{A_n} = \left[\frac{1 + \frac{1}{2} (\gamma - 1) M_{n+1}^2}{1 + \frac{1}{2} (\gamma - 1) M_n^2} \right]^{\frac{1}{\gamma-1}} \left[\frac{1}{M_n^2} \frac{M_{n+1}^2 - M_n^2}{1 + \frac{1}{2} (\gamma - 1) M_{n+1}^2} + 1 \right]^{-\frac{1}{2}} \quad (11)$$

The area of the spherical cap cut by a cone with its apex at the center of the sphere is

$$A_s = \int_0^{\alpha_n} 2\pi R^2 \sin \phi \, d\phi = 2\pi R^2 (1 - \cos \alpha_n), \quad (12)$$

and the plane area corresponding to the base of this cone is

$$A_p = \pi R^2 \sin^2 \alpha_n. \quad (13)$$

Consequently, the relationship between the plane and the spherical areas is

$$A_p = \frac{A_s (1 + \cos \alpha_n)}{2} \quad (14)$$

Since the plane area A_p is proportional to the square of the radius r^2 , Equation 11 and 14 may be combined to yield an expression for the ratio of the radii at the points n and $n + 1$.

$$\frac{r_{n+1}}{r_n} = \left(\frac{A_{n+1}}{A_n} \right)^{\frac{1}{2}} .$$

The term on the right in Equation 11 can be simplified considerably by identifying it as the isentropic ratio, $(A/A^*)_{n+1}/(A/A^*)_n$ where

$$\frac{A}{A^*} = \frac{1}{M} \left[\left(\frac{2}{\gamma+1} \right) \left(1 + \frac{\gamma-1}{2} M^2 \right) \right]^{\frac{\gamma+1}{2(\gamma-1)}} \quad (15)$$

Equation 11 may now be written as

$$\frac{r_{n+1}}{r_n} = \left[\frac{(1 + \cos \alpha_{n+1})(A/A^*)_{n+1}}{(1 + \cos \alpha_n)(A/A^*)_n} \right]^{\frac{1}{2}} . \quad (16)$$

Latvala provides the following relation for the jet boundary:

$$dX/dr = \cot \alpha . \quad (17)$$

This equation cannot be solved explicitly, but it can be solved easily if the method of finite differences is used. When ΔX , Δr , and $\Delta \alpha$ are restricted to small values, Equation 17 is

$$\frac{\Delta X}{\Delta r} = \cot \left(\alpha_n - \frac{\Delta \alpha}{2} \right) \quad (18)$$

since $\Delta r = r_{n+1} - r_n$,

$$\frac{\Delta X}{r_n} = \left(\frac{r_{n+1}}{r_n} - 1 \right) \cot \left(\alpha_n - \frac{\Delta \alpha}{2} \right) . \quad (19)$$

The fundamental Equations, 16 and 19, for describing jet plume boundaries may be written in dimensionless form by dividing by the exit radius of the nozzle,

$$\frac{r_{n+1}/r_e}{r_n/r_e} = \left[\frac{(1 + \cos \alpha_{n+1})(\Lambda/\Lambda^*)_{n+1}}{(1 + \cos \alpha_n)(\Lambda/\Lambda^*)_n} \right]^{\frac{1}{2}} \quad (20)$$

$$\frac{\Delta X/r_e}{r_n/r_e} = \left(\frac{r_{n+1}/r_e}{r_n/r_e} - 1 \right) \cot \left(\alpha_n - \frac{\Delta \alpha}{2} \right). \quad (21)$$

The initial expression of the axisymmetric underexpanded jet is determined from the P-M equation for turning angle.

Each spherical surface in the flow stream has associated with it an average Mach number, P-M angle, and isentropic area ratio. If it is assumed that the average turning angle of the jet flow stream is the same as the change in the P-M angle between two closely spaced surfaces, the entire boundary may be calculated in a sequential manner.

Since ν is known, M_1 and A_1/Λ^* may be calculated or found in tables of isentropic flow functions for different values of γ . Choosing a $\Delta \alpha$ and adding it to ν_1 will then give a value for ν_2 . Corresponding to this second P-M angle, there will be a Mach number M_2 and area ratio A_2/Λ^* . This information, used in Equations 20 and 21, is sufficient to calculate r_2/r_e and $\Delta X/r_e$ (since $\alpha_2 = \alpha_1 - \Delta \alpha$). A point, $n = 3$, might now be determined by adding $\Delta \alpha$ to ν_2 to obtain ν_3 and continuing the step-by-step approach until an adequate portion of the boundary has been calculated.

Latvala suggests that, for highly underexpanded jets, α may be varied in increments of approximately 5 degrees for the first few points and then in increments of about 1 degree for the remainder of the calculations with very good results. Boundaries computed by the method of characteristics as presented by Love (Ref. 11) have been

compared with the results of Latvala (Ref. 10) and compare quite favorably with the more exact results.

THE CIRCULAR-ARC APPROXIMATION

During an experimental investigation at the Arnold Engineering Development Center (Ref. 12), it was found that the initial portion of the jet boundary from the nozzle lip to the point of maximum jet diameter could be approximated by a circular arc. For a particular Mach number and specific heat ratio, the radii of the boundaries are practically invariant with the ratio of chamber pressure to ambient pressure. A plot of jet boundary radius ratio R/r_c as a function of Mach number for $\gamma = 1.4$ measured from a large number of Schlieren photographs is given in Figure 11. To use Figure 11 for approximating jet boundaries, the initial inclination angle must be determined. This can be found from Equation 1. With the initial angle known, a line is drawn normal to the tangent of α at the nozzle lip, the radius R is located on this line, and the boundary can be drawn with a compass.

The radius ratio varies approximately as a^*/V_c . If a similar variation of R/r_c as a function of M_c is assumed for any other specific heat ratio, Figure 11 and the following equation can be used to obtain the radius ratio for other values of the specific heat ratio.

$$\left(\frac{R}{r_c}\right) = \left(\frac{R}{r_c}\right)_{\text{air}} \left[\frac{(V_c/a^*)}{(V_c/a^*)_{\text{air}}} \right] = \left(\frac{R}{r_c}\right)_{\text{air}} \left[\frac{(\gamma + 1)(5 + M_c^2)}{12 \left(1 + \frac{\gamma + 1}{2} M_c^2\right)} \right]^{\frac{1}{2}}$$

The subscript "air" refers to values of R/r_c for $\gamma = 1.4$ taken from Figure 11. Jet boundaries for $\gamma = 5/3$ calculated by the method of characteristics are plotted in Figure 12. Circular-arc approximations using Equations 1 and 22 and Figure 11 are also shown. At higher pressure ratios circular-arc approximation fits the method-of-characteristics solution quite well. Comparisons with experimental results are also favorable.

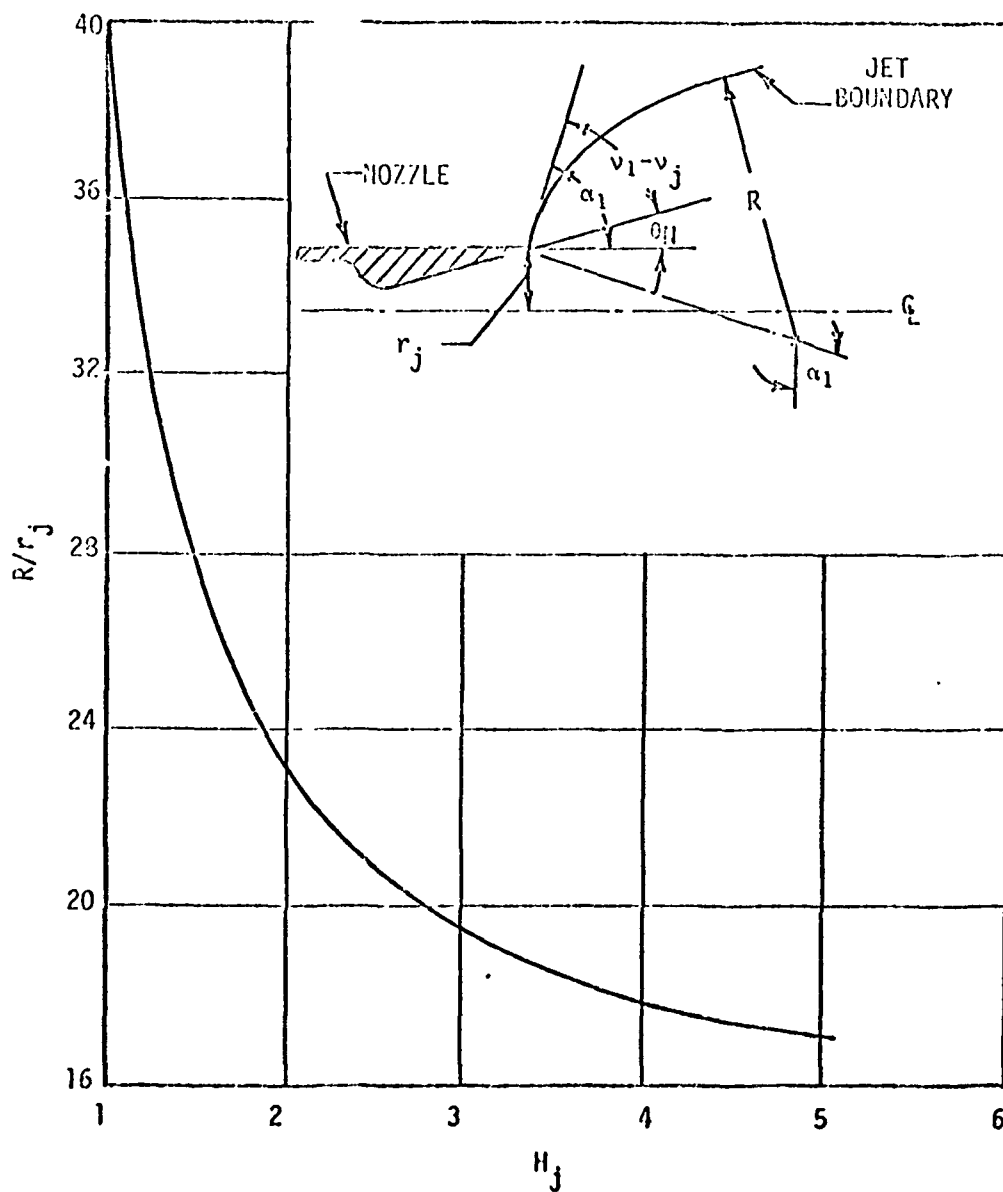


FIGURE 11. RADIUS RATIO OF JET BOUNDARY FOR $\gamma = 1.4$ (FROM REF. 10)

REPRODUCIBILITY OF THE ORIGINAL PAGE IS POOR

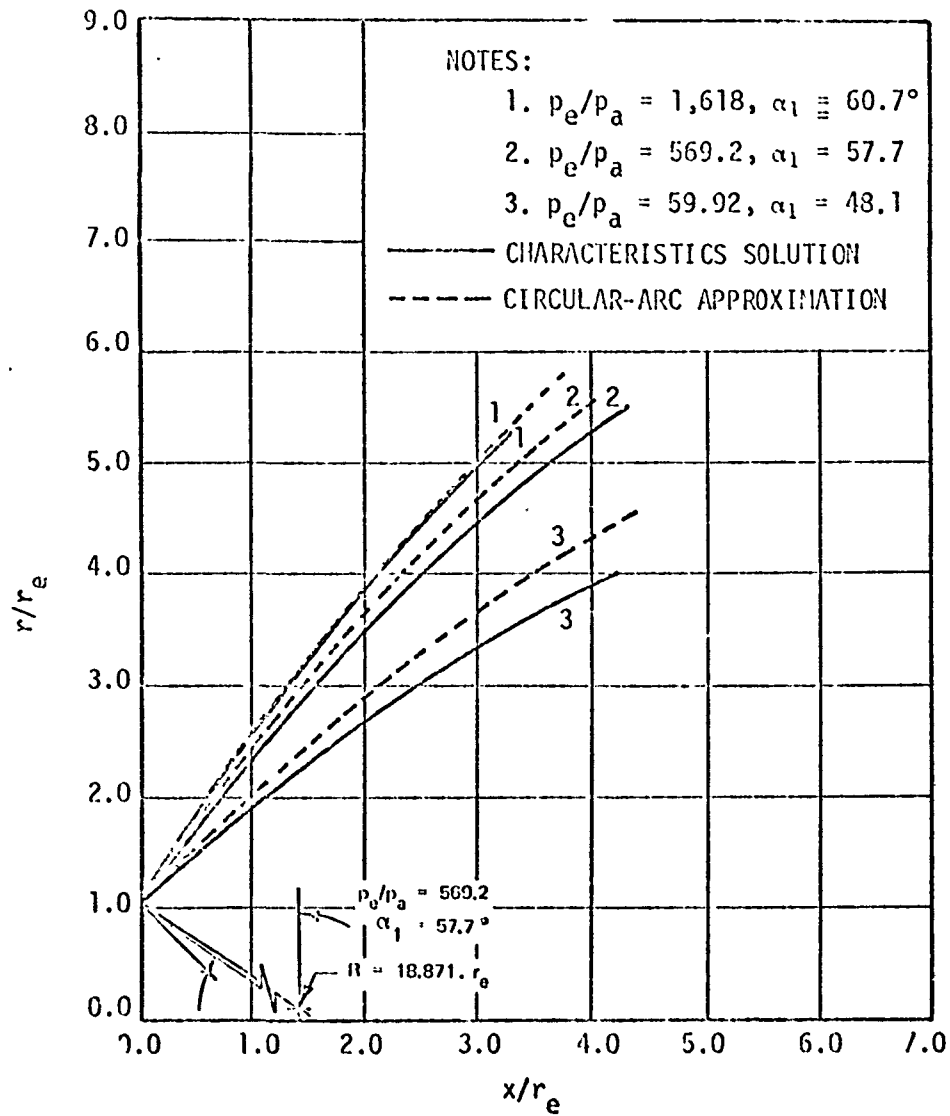


FIGURE 12. CIRCULAR-ARC APPROXIMATION COMPARED WITH METHOD-OF-CHARACTERISTICS SOLUTION (FROM REF. 10)

Latvala (Ref. 10) comments that it is somewhat surprising that the simple physical model used in the derivation of the method fits the experimental and theoretical results as well as it does. The jet flow is, of course, highly irreversible and contains a complicated multi-dimensional shock structure, although the isentropic assumption is implicitly used in the derivation. Nevertheless, the empirical nature of the method does not detract from its value as a convenient method of quickly estimating the initial portion of jet boundaries.

For all of the approximations discussed here, the gas composition at the exit plane and beyond is fixed. The isentropic flow relations are also assumed to be valid in the interior of the plume. Static pressure and temperature can be expressed as functions of the local plume Mach number and the nozzle exit conditions

$$T = \frac{T_e \{1 + [(\gamma - 1)/2] M_c^2\}}{1 + [(\gamma - 1)/2] M^2}$$

$$P = P_e (T/T_e)^{\frac{\gamma}{\gamma - 1}}$$

Mach number distributions would be of more general use if they were available in analytical form. French (Ref. 8) has reported an analytical approximation to the method-of-characteristics computer solution, which represents the Mach number distribution fairly well. The expression is

$$M(\sigma, X) = \frac{B(\sigma^2 - 1)}{X} + DX + E$$

where $\sigma = r/r_e$ and $X = x/r_e$. The nature of discrepancies caused by using this approximation may be found in the paper by French (Ref. 8).

THE PSEUDO-NOZZLE APPROXIMATION

Luce and Jarvinen (Ref. 13) have suggested an approximate method of describing the underexpanded flow from a nozzle into still air.

Two assumptions form the basis for their treatment. The following function is chosen to represent the contact surface in parametric form:

$$\frac{r}{r_m} = \frac{5}{4} \left[\left(\frac{x}{x_m} \right)^{\frac{1}{2}} - \frac{1}{5} \left(\frac{x}{x_m} \right)^{\frac{5}{2}} \right] \quad (23)$$

Application of conservation of momentum at the nozzle exit and the point of maximum diameter in the lateral and axial directions provides equations relating x_m and r_m . This procedure considers force equal to the difference in thrusts of ideal nozzles of exit areas A_e and A_m . The maximum radial coordinate may be found from the following equation:

$$(p_a/p_c)(A_m/A_e) = C_{F_m} - C_{F_e} \quad (24)$$

where C_{F_m} is the thrust coefficient at the point (r_m, x_m) . Since $A_m = \pi r_m^2$, one coordinate is immediately known.

Hill and Haber (Ref. 14) have discussed the approximation,

$$C_{F_m} = C_{F_{max}} \quad (25)$$

and state that it provides an error of less than 1 percent for altitudes above 100 kilometers.

The approximation is of considerable value since $C_{F_{max}}$ is a function only of the ratio of specific heats of the exhaust product mixture,

$$C_{F_{max}} = \frac{2\gamma}{(\gamma^2 - 1)^{\frac{1}{2}}} \left(\frac{2}{\gamma + 1} \right)^{\frac{1}{\gamma - 1}} \quad (26)$$

The vacuum thrust coefficient at the nozzle exit is also available from isentropic flow relations.

$$C_{F_e} = \left\{ \frac{2\gamma^2}{\gamma - 1} \left(\frac{2}{\gamma + 1} \right)^{\frac{\gamma + 1}{\gamma - 1}} \left[1 - \left(\frac{p_e}{p_c} \right)^{\frac{\gamma - 1}{\gamma}} \right] \right\}^{\frac{1}{2}} + \frac{A_e}{A_e} \frac{p_e}{p_c} \quad (27)$$

An approximate yet very direct way of obtaining x_{11} may be deduced from the conclusions of Luce and Jarvinen (Ref. 13). The data they considered seemed to indicate that x_{11}/r^* is essentially independent of γ and ϵ and is only a function of p_c/p_a . A straight line applicable for this relation yields

$$\log_{10} \left(\frac{r_{11}}{r^*} \right) = 0.55 \log_{10} \left(\frac{p_c}{p_a} \right) - 0.1. \quad (28)$$

The use of such an empirical expression should not be judged for physical meaning. It is expected to provide reasonable results for ratios of (r_{11}/r^*) and (p_c/p_a) greater than ten.

An actual definition of the space cone of a jet plume at high altitudes may be based on the percentage of mass flow within a given conical region. The far field of a jet is essentially radial flow, with straight streamlines appearing to originate from a common source. The stream density ρV varies along each streamline as $1/r^2$. The flow may be described by specifying the mass flux per unit solid angle

$$dm/d\Omega = \rho V r^2$$

as a function of the angle ϕ between a given streamline and the axis of a jet. The rapid decay of $dm/d\Omega$ away from the axis (see Figures 3 and 6) may be approximated by members of the one-parameter family

$$\frac{(dm/d\Omega)_\phi}{(dm/d\Omega)_{\phi=0}} = \exp[-\lambda^2 (1 - \cos \phi)^2]. \quad (29)$$

The value of λ has been determined by Hill and Draper (Ref. 15) to be

$$\lambda = [(\pi)^{\frac{1}{2}} (1 - C_F/C_{F_{\max}})]^{-1}. \quad (30)$$

Specification of γ and Λ/A^* fixes $C_F/C_{F_{\max}}$ (refer to Equations 26 and 27). The value of λ then varies from one constant-property to the next because of the variation in the Crocco number, $C = V/V_m$.

COMMENTS

The approximations discussed in the previous section are only a few of the many proposed schemes. These have been selected to illustrate methods that are difficult, in the sense of being time consuming, and easy in the sense of being very rapid. The circular-arc and pseudo-nozzle approximations are in the easy category.

It is possible that the space plumes illustrated in Figures 3 and 6 will prove to be sufficient for the information needed on space plume boundaries and flow-field properties. If this should prove not to be so, further approximate descriptions may be generated. There is some application of the methods discussed to the general problem of particles ejected from a space vehicle. In many ways such a stream can be considered as the exhaust of a jet and described as flow from a point source.

PARTICLE FIELD INTERACTIONS

As part of our studies in particle field interactions, a report has been published on spacecraft-ionosphere interactions (Ref. 19). Efforts to improve the analysis by Newkirk (Ref. 16) of debris cloud formation have indicated some shortcomings in his assumptions. Planned efforts in predicting the degradation of radiation received by ATM experiments are discussed and described in this section.

DWELL-TIME AND PARTICLE DISTRIBUTION

Particle lifetime has been defined by Newkirk (Ref. 16) as the time required for aerodynamic drag to stop (relative to a space vehicle) the particle which had been initially ejected in the forward direction. The lifetime is used to calculate the radius of the debris cloud by taking the sum of the radius of the spacecraft and the product of the ejection velocity and the lifetime,

$$R_M = R_S + u_0 \tau \quad (31)$$

where

- R_M - the radius of the debris cloud
- R_S - the radius (or characteristic length) of the space vehicle
- u_0 - the ejection velocity
- τ = u_0 / \dot{u} is the lifetime, where \dot{u} is the deceleration.

Within the cloud, the distribution of particles is taken to be

$$n(r) \approx r^{-\delta}$$

where

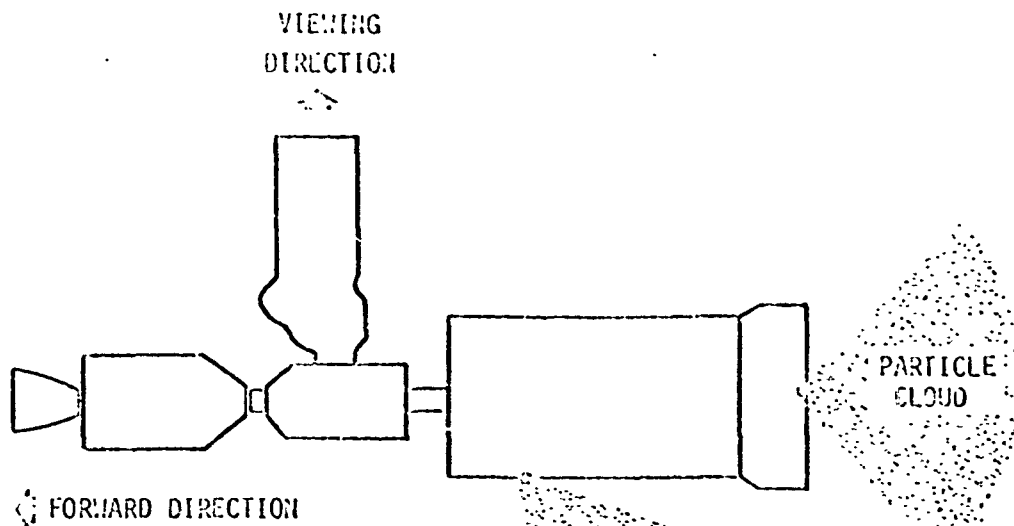
$n(r)$ - the number of particles per unit volume

r - the radial coordinate measured from the spacecraft center

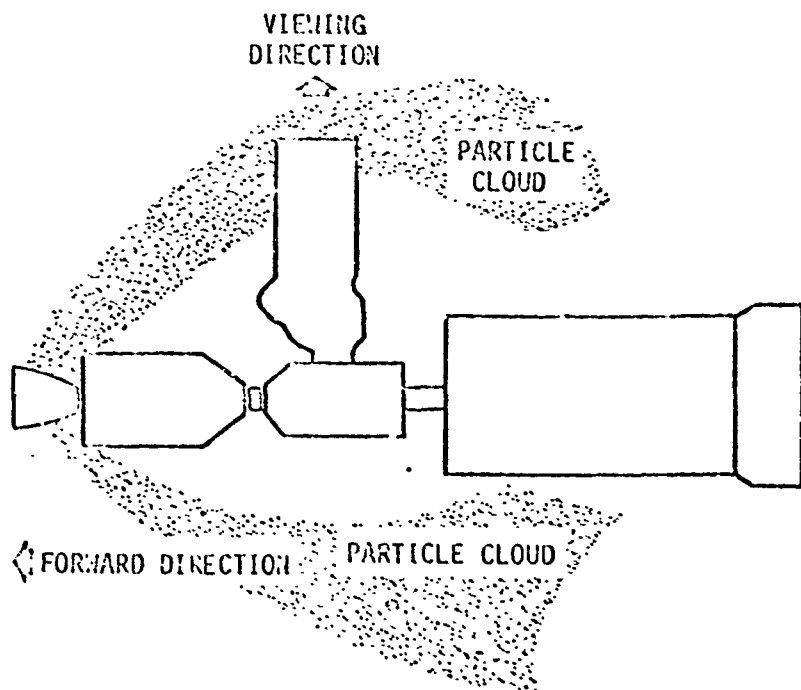
δ - a small positive number (≈ 3).

This estimation is based on considerations of distributions found in natural aerosols and in droplets produced by atomizers.

The validity of brightness estimates of the debris cloud resulting from the above assumptions is not immediately suitable for testing since all of these assumptions are far from being realistic. Refinements of lifetimes, however, for RCS ejected particles are presented in Appendix E. For example, the only use of lifetime is to calculate the radius of the cloud; but there is a question, however, as to whether the cloud really has a radius. The shape of the cloud and the distribution of particles within the cloud depend completely on the direction as well as magnitude of ejection velocity of each particle and the position on the spacecraft from which the particle emanates. If the viewing direction and direction of motion of the orbital complex is as shown in Figure 13, particles ejected from certain regions with velocity less than that of the cluster will, in general, have no way to reach a position near the observing port. Rocket exhaust plumes, however, with very high particle velocities, may reach back to produce threatening material in the vicinity of the experiments. The optical viewing direction may be more susceptible to particulate contamination from certain directions than would be expected from a spherically symmetric cloud. Much more dangerous sample source regions are also indicated in Figure 13.



(A) SAMPLE SOURCES OF NONINTERFERING PARTICLES



(B) SAMPLE SOURCES OF INTERFERING PARTICLES

FIGURE 13. PARTICLE SOURCE REGION

To evaluate optical contamination effects due to a cloud of ejected particles, the use of lifetime as suggested by Newkirk is not of much value. Instead in a coordinate system fixed at a central point of the space vehicle of principal interest, one should know:

- o The position of the optical equipment; x_0, y_0, z_0
- o The position at which a particle is ejected; x_i, y_i, z_i
- o The velocity with which a particle is ejected; u_i, v_i, w_i
- o An optical range, $F =$ a set of (x, y, z) , which is the field of view of the optical equipment.

Any velocity is represented as $\vec{u} = (u, v, w)$ in the chosen coordinate system. These parameters, illustrated in Figure 14, are all necessary to determine the distribution. If these are known, one could, in principle, determine the particle distribution within the optical range F according to a given rate of ejection of the particles of a specified type $(x_i, y_i, z_i; u_i, v_i, w_i)$. This, of course, is beyond the range of present practicality because of the number of particles involved.

As an example of the different points of view, consider an oil-burning car which gives out black smoke while running. The optical effects as observed by a man seated in the car can be investigated only when the following are known:

- o The location of the opening of the exhausting pipe (x_i, y_i, z_i)
- o The location of the eyes of the observer or whatever equipment used (x_0, y_0, z_0)
- o The rate at which the black smoke is ejected.
- o The field of view of the observer (F)
- o The particle velocity (u_i, v_i, w_i) .

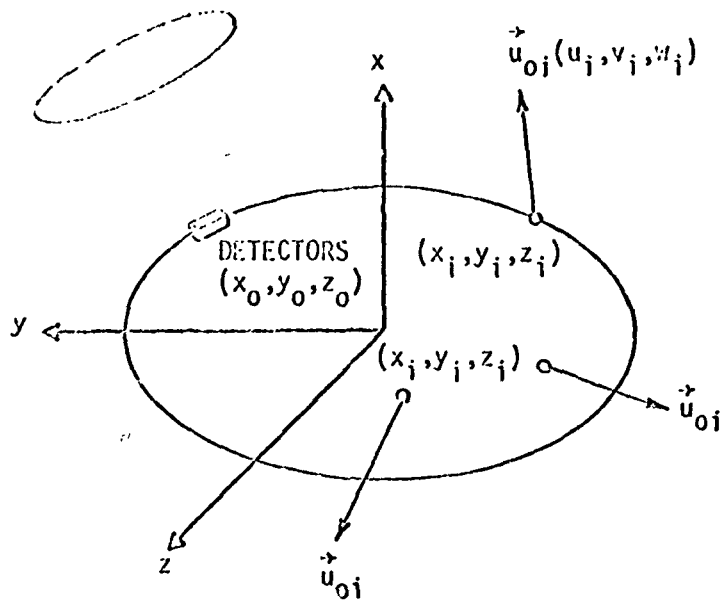


FIGURE 14. PARAMETERS FOR DESCRIPTION OF PARTICLES IN DEBRIS CLOUD

The optical effect is determined by calculating the distribution of smoke particles within R. Using Newkirk's treatment, without the above information, involves treating the car as a sphere and predicting that the smoke surrounding the car will form a spherical cloud.

OPTICAL INTERFERENCE BY DEBRIS CLOUD

An alternative method of evaluating the threat of optical contamination to an ATM mission by particles ejected from the cluster is to calculate the effects of a collection of particles located in front of and near the observing equipment. A comparison between the amount of material in such a cloud which causes degradation and the possible sources and transport schemes of such ejecta to the sensitive regions should demonstrate the magnitude of the contamination threat.

A project has been started to calculate the optical effects of a debris cloud in the vicinity of the ATM experiment using available theory.

Assorted materials are known to emanate from space vehicles. These include gaseous components and liquid and solid particles. Water is expected to be the most abundant material, in the form of droplets or crystals. The particle size which may cause the most interference with optical experiments is in the range of 0.1 to 100 microns.

There are two basic effects of the debris cloud particles on optical observations. The first effect may be called "background radiation." When cloud particles are illuminated by a radiation source other than the object source, part of the radiation will be scattered into the optical detecting equipment, thus contributing a background radiation

superimposed on that from the object source. The second effect is that of absorption and/or extinction which may be called attenuation. Radiation from an object source will be attenuated by particles interposed between the source and the detectors. The received radiation at the ATM will be composed of source and background radiation reduced by the cloud attenuation.

FUTURE PLANS

Since there is not yet sufficient information on the particle density and velocity distributions of the ATM debris cloud, the cloud will be described by a set of free parameters. For example, the particle concentration or dimensions of the cloud may be allowed to vary over a proper and reasonable range. Calculations will be made for:

- o Rayleigh scattering, applicable to gaseous components
- o Mie scattering, applicable to particulate matter in the infrared range
- o Geometric optics, applicable to particulate matter in the visible, ultraviolet, and X-ray regions.

The ultimate purpose is to obtain functions describing background radiation and attenuated radiation in terms of parameters characterizing the debris cloud.

APPENDIX A. ANALYSIS OF AN IDEAL ROCKET

Chemical rockets consist of a great variety of simple and complex propellant supply and feed systems, a combustion chamber, and an exhaust nozzle. For the analysis of an ideal rocket engine, the following assumptions are made:

- The working fluid is a perfect gas of constant composition.
- The chemical reaction is equivalent to a constant-pressure heating process.
- The expansion process is steady, one-dimensional, and isentropic.

The thrust chamber may now be described qualitatively with the aid of a temperature as a function of entropy (T as a function of s) diagram as shown in Figure A-1. Propellant enters at State 1. A quantity of heat Q_R (the heating value of the propellant combination per unit mass) is added at constant pressure, and the propellant reaches the nozzle inlet at State 2. The propellant expands isentropically from State 2 through the throat, where the Mach number is unity, to the exhaust where the velocity is M_0 . Conservation of energy applied to the heating process yields

$$\dot{m}(h_{02} - h_{01}) = \dot{m}c_p(T_{02} - T_{01}) \quad (\text{A-1})$$

or

$$T_{02} = T_{01} + Q_R/c_p \quad (\text{A-2})$$

where

\dot{m} - the propellant mass flow rate

c_p - the specific heat at constant pressure

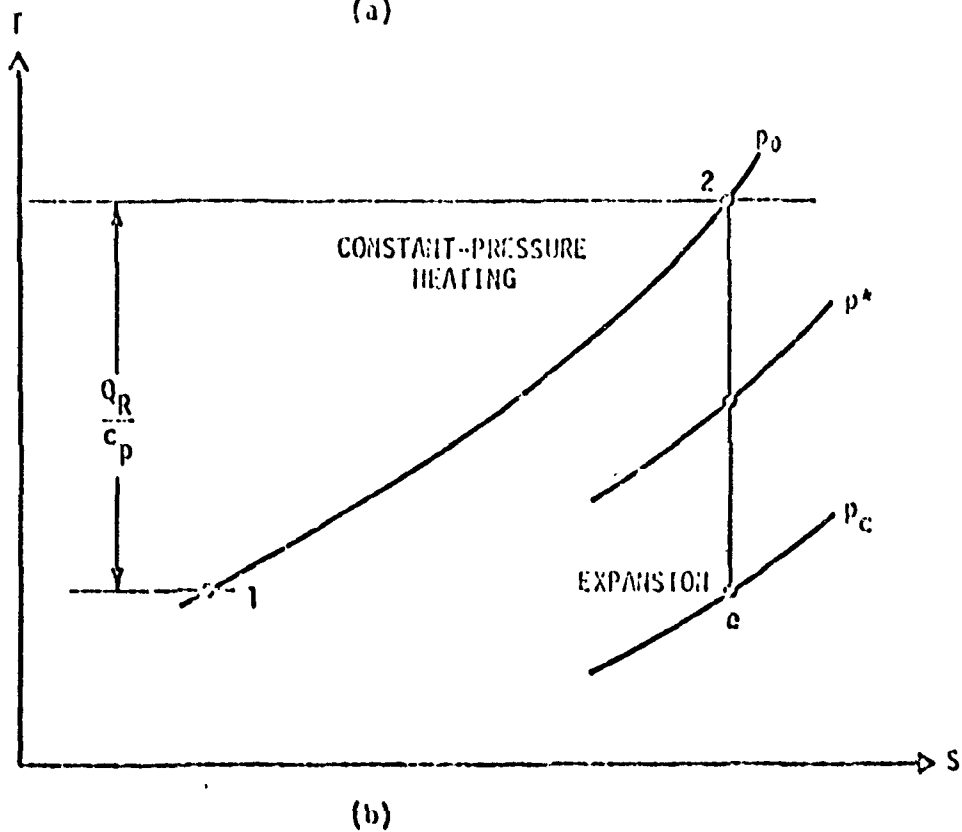
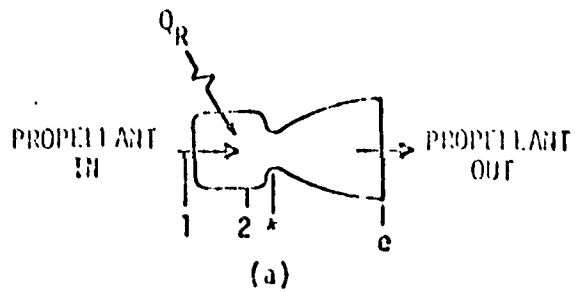


FIGURE A-1. SIMPLE ROCKET THRUST CHAMBER (FROM REF. 10)

h - enthalpy

o - refers to stagnation conditions.

Under the assumption of adiabatic nozzle expansion, the energy equation requires constant stagnation enthalpy in the nozzle:

$$h_{02} = h_{00} \quad (\Lambda-3)$$

or

$$u_0^2/2 = h_{02} - h_o = c_p(T_{02} - T_o) \quad (\Lambda-4)$$

If the expansion is isentropic, then the theory of steady one-dimensional flow of a perfect gas provides a useful series of relations. The exit velocity is

$$u_o = \left\{ 2 c_p T_{02} \left[1 - (p_o/p_{02})^{(\gamma-1)/\gamma} \right] \right\}^{1/2} \quad (\Lambda-5)$$

where p is the pressure and γ is the ratio of specific heat at constant pressure to specific heat at constant volume. Expressing c_p in terms of γ , the universal gas constant \bar{R} and the propellant molecular weight \bar{M} , the exit velocity may be written as

$$u_o = \left\{ \frac{2\gamma\bar{R}}{(\gamma-1)\bar{M}} T_{02} \left[1 - \left(\frac{p_o}{p_{02}} \right)^{(\gamma-1)/\gamma} \right] \right\}^{1/2} \quad (\Lambda-6)$$

The propellant mass flow rate \dot{m} is also derived from isentropic flow equations and is given in terms of the properties of the combustion-chamber fluid and the nozzle throat area Λ^* by:

$$\dot{m} = \frac{\Lambda^* p_{02}}{(R T_{02})^{1/2}} \left[\gamma \left(\frac{2}{\gamma+1} \right)^{(\gamma+1)/(\gamma-1)} \right]^{1/2} \quad (\Lambda-7)$$

where $R = \bar{R}/\bar{M}$.

For isentropic flow, another quantity of interest, the exhaust pressure p_o may be found in terms of the expansion ratio $\epsilon = \Lambda_o/\Lambda^*$.

The thrust of a simple chemical rocket engine may be written as

$$T = \dot{m} u_e + (p_e - p_a) A_e \quad (\text{A-8})$$

where p_a is ambient pressure.

Substituting from equations for u_e and \dot{m} , we obtain the following expression:

$$\frac{T}{A^* p_0} = \left\{ \frac{\gamma \gamma^2}{\gamma - 1} \left(\frac{\gamma}{\gamma + 1} \right)^{\frac{\gamma + 1}{\gamma - 1}} \left[1 - \left(\frac{p_e}{p_0} \right)^{\frac{\gamma - 1}{\gamma}} \right] \right\}^{\frac{1}{2}} + \left(\frac{p_e}{p_0} - \frac{p_a}{p_0} \right) \epsilon \quad (\text{A-9})$$

where $p_0 = p_{02}$ is the stagnation pressure of the combustion chamber.

The ideal rocket provides a basis for comparison of real and ideal rockets. To describe the performance of each component of the thrust chamber, two coefficients are defined. For the combustion chamber the characteristic velocity c^* is defined as

$$c^* = \frac{p_0 A^*}{\dot{m}} \quad (\text{A-10})$$

This can be written as, using Equation A-9,

$$c^* = \left[\frac{1}{\gamma} \left(\frac{\gamma + 1}{\gamma} \right)^{\frac{\gamma + 1}{\gamma - 1}} R T_0 \right]^{\frac{1}{2}} \quad (\text{A-11})$$

For the nozzle, the thrust coefficient is defined as

$$C_F = \frac{T}{p_0 A^*} \quad (\text{A-12})$$

From Equation A-9, C_F is given by

$$C_F = \left\{ \frac{\gamma \gamma^2}{\gamma - 1} \left(\frac{\gamma}{\gamma + 1} \right)^{\frac{\gamma + 1}{\gamma - 1}} \left[1 - \left(\frac{p_e}{p_0} \right)^{\frac{\gamma - 1}{\gamma}} \right] \right\}^{\frac{1}{2}} + \frac{p_e - p_a}{p_0} \epsilon \quad (\text{A-13})$$

The combination of equations yields

$$\Gamma = \dot{m} c^* C_p . \quad (\text{A-11})$$

Comparison of c^* and C_p calculated from Equations A-10 and A-12 with ideal values from Equations A-11 and A-13 indicate how well each component is performing.

The ideal nozzle flow can be refined slightly to account, in the case of conical nozzles, for the effect of nonaxial exhaust velocities. For the flow illustrated in Figure A-2, it is assumed that the streamlines in the expanding part of the nozzle are straight lines which all intersect at the Point O. A control surface is indicated, passing through the spherical segment (of radius R) over which the exhaust properties are constant. The reaction to the thrust is shown as the vector T. The application of the conservation of momentum to this control volume yields

$$\sum F_x = \Gamma + (p_a - p_e) A_e = \int \rho (\mathbf{u} \cdot \mathbf{n}) u_x dA \quad (\text{A-15})$$

for components of force in the axial (x) direction. Here F is force, ρ is density, \mathbf{n} is a unit normal vector, and A_e , the plane exhaust area, equals πr^2 . No mass crosses the control surface except over the spherical exhaust segment where

$$dA = 2\pi R \sin \phi R d\phi . \quad (\text{A-16})$$

In addition

$$\vec{\mathbf{u}} \cdot \vec{\mathbf{n}} = u_0 \quad \text{and} \quad u_x \cos \phi . \quad (\text{A-17})$$

The angle ϕ is defined in Figure A-2. The equation may be written for the thrust.

$$\Gamma = \int_0^\alpha \rho (u_e) u_e \cos \phi 2\pi R^2 \sin \phi d\phi + (p_e - p_a) A_e . \quad (\text{A-18})$$

REPRODUCIBILITY OF THE ORIGINAL PAGE IS POOR

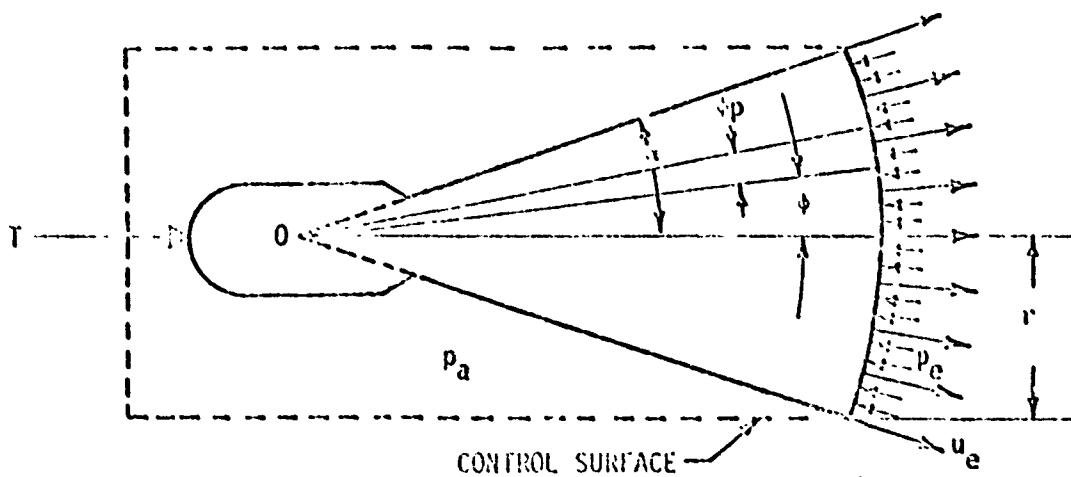


FIGURE A-2. SPHERICALLY SYMMETRIC NOZZLE FLOW (FROM REF. 20)

The integration yields

$$\Gamma = 2\pi R^2 \rho u_e^2 \frac{1 - \cos^2 \alpha}{2} + (p_e - p_a) \Lambda_e'. \quad (A-19)$$

Since the area of the spherical exhaust segment Λ_e' is $2\pi R^2(1 - \cos \alpha)$, the propellant flow rate is

$$\dot{m} = \rho u_e \cdot 2\pi R^2 (1 - \cos \alpha). \quad (A-20)$$

The thrust may then be approximated as

$$\Gamma = \frac{1 + \cos \alpha}{2} \dot{m} u_e + (p_e - p_a) \Lambda_e \quad (A-21)$$

where Λ_e' has been replaced by Λ_e . This result shows that the thrust of an ideal conical rocket of half angle α is reduced by a factor λ

$$\lambda = \frac{1 + \cos \alpha}{2} \quad (A-22)$$

over that of an axial-outlet rocket with the same exhaust conditions.

The performance of a real nozzle is further reduced by frictional effects. This may be represented by an empirical discharge coefficient C_d such that

$$C_F(\text{actual}) = C_d \lambda C_F(\text{ideal}). \quad (A-23)$$

APPENDIX B. REACTION CONTROL SYSTEM ENGINE CHARACTERISTICS

The characteristics of two RCS engines are presented in Table B-1. The fuels used are either monomethylhydrazine (MMH) or a mixture of 50-percent unsymmetrical dimethylhydrazine (UDMH) and 50-percent hydrazine (N_2H_4). The characteristic velocity is denoted by c^* . Subscripts c and e are used to indicate chamber and exit plane conditions, respectively. The mean molecular weight of the fuel-oxidizer mixture is \bar{M} . Throat diameter and nozzle exit diameter are D_t and D_e , respectively. The angle θ_c is the contraction half angle. The nozzle expansion half angle is θ_N . Exit Mach numbers are calculated using the following formula,

$$M_e = \frac{I_{sp} g_0}{(\gamma R T)^{1/2}}$$

where g_0 , the acceleration of gravity, is a conversion factor. The primary method of cooling nozzle walls is also given in Table B-1. Other methods are also used to some extent.

Exhaust compositions for the three RCS engines are given in Tables B-2 and B-3. The values are required to calculate the interference of a debris cloud with incoming radiation. The engine dimensions, particularly illustrating nozzle sizes, are shown in Figure B-1.

TABLE B-1. CHARACTERISTICS OF TWO RCS THRUSTER ENGINES

Item	RCS Characteristics	
	CM	SM-LM
Thrust, lb	100	100
Fuel	N ₂ O ₄ /NPH	N ₂ O ₄ /50-50
Thrust coefficient	1.81	1.75
Specific impulse, sec	286	280
Characteristic velocity (C*), ft/sec	5,100	5,149
Flow rates, lb/sec		
N ₂ O ₄	0.219	0.239
Fuel	0.137	0.118
Chamber pressure, psi	126	97
Chamber exit plane, psi	0.19	0.162
Chamber temperature, °K	2,540	2,800
Exit plane temperature, °K		
Chamber mean molecular weight	20.58	23.13
Exit plane mean molecular weight	20.62	23.33
Chamber ratio of specific heats	1.211	1.153
Exit plane ratio of specific heats	1.337	1.287
Throat diameter, in.	0.755	0.868
Throat area, in ²	0.448	0.592
Exit plane diameter, in.	4.78	5.46
Exit plane area, in ²	17.92	23.41
Area expansion ratio	40	40
Contraction half angle, deg	45	53
Nozzle half angle, deg	17	8
Exit plane Mach number	4.69	4.31
Cooling	ablation	radiation

TABLE B-1. CHARACTERISTICS OF TWO RCS THRUSTER ENGINES

Item	RCS Characteristics	
	CM	SM-LM
Thrust, lb	100	100
Fuel	N ₂ O ₄ /NPH	N ₂ O ₄ /50-50
Thrust coefficient	1.81	1.75
Specific impulse, sec	286	280
Characteristic velocity (C*), ft/sec	5,100	5,149
Flow rates, lb/sec		
N ₂ O ₄	0.219	0.239
Fuel	0.137	0.118
Chamber pressure, psi	126	97
Chamber exit plane, psi	0.19	0.162
Chamber temperature, °K	2,540	2,800
Exit plane temperature, °K		
Chamber mean molecular weight	20.53	23.13
Exit plane mean molecular weight	20.62	23.33
Chamber ratio of specific heats	1.211	1.153
Exit plane ratio of specific heats	1.337	1.287
Throat diameter, in.	0.755	0.868
Throat area, in ²	0.448	0.592
Exit plane diameter, in.	4.78	5.46
Exit plane area, in ²	17.92	23.41
Area expansion ratio	40	40
Contraction half angle, deg	45	53
Nozzle half angle, deg	17	8
Exit plane Mach number	4.69	4.31
Cooling	ablation	radiation

TABLE B-2. EXHAUST COMPOSITIONS, CH-RCS ENGINE

<u>Component</u>	<u>Composition (mole %)</u>	
	<u>Chamber</u>	<u>Exit</u>
H ₂ O	33.6	33.5
N ₂	30.9	31.0
H ₂	17.6	18.0
CO	13.1	12.9
CO ₂	4.0	4.3
OH	0.2	Trace*
H	0.4	0.002
NO		Trace
O ₂		Trace

* A trace is less than 0.0006 percent.

TABLE B-3. EXHAUST COMPOSITIONS, LH/SM-RCS ENGINE

<u>Component</u>	<u>Composition (mole %)</u>	
	<u>Chamber</u>	<u>Exit</u>
H ₂ O	43.62	44.88
N ₂	35.04	35.42
CO ₂	7.17	7.76
CO	5.54	5.06
H ₂	4.95	4.55
OH	1.82	1.19
H	0.708	0.484
O ₂	0.57	0.32
NO	0.42	0.25
O	0.16	0.070

REPRODUCIBILITY OF THE ORIGINAL PAGE IS POOR.

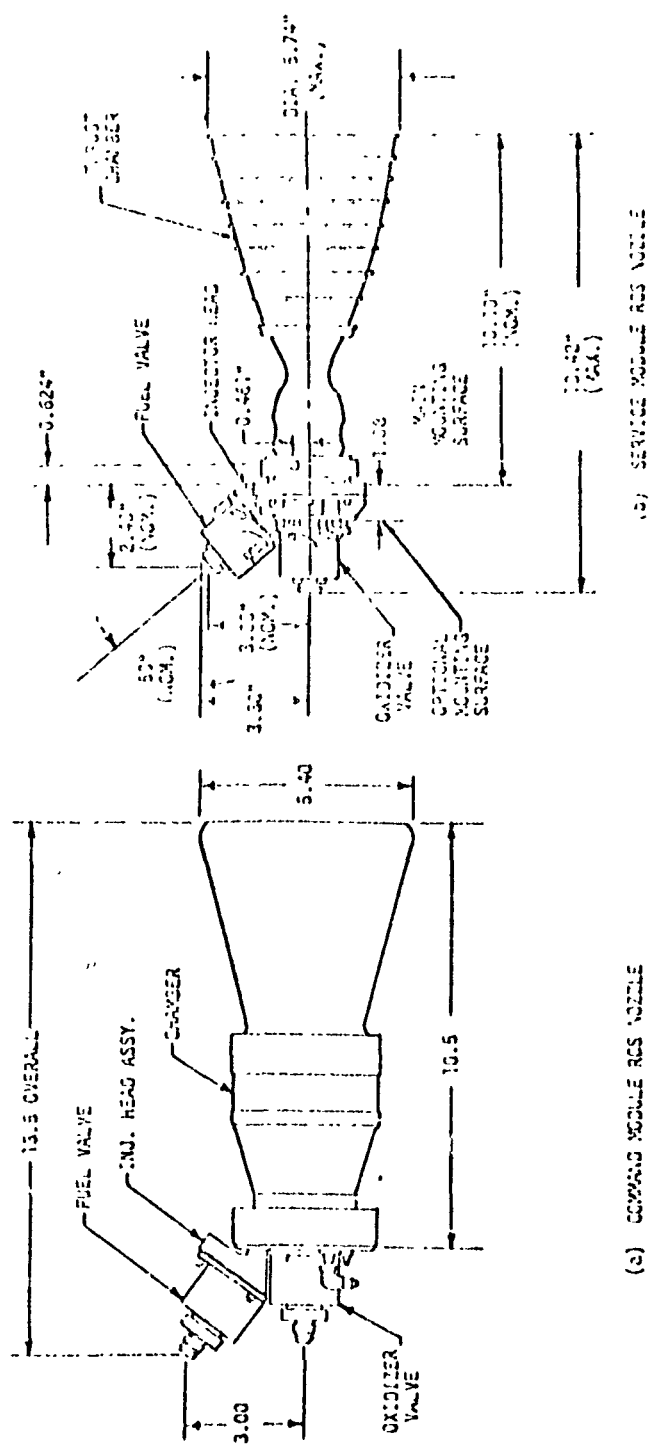


FIGURE B-1. RCS NOZZLES (FROM REF. 1)

APPENDIX C. RCS PARTICLE LIFETIME

Newkirk (Ref. 16) defines the lifetime of a particle in the vicinity of a spacecraft as

$$\tau = u_0 / \dot{u}$$

where u_0 is the initial particle velocity when leaving the spacecraft, and \dot{u} is the acceleration of particles away from the spacecraft.

The velocity of a typical particle in the exit plane of an RCS thruster nozzle may be estimated as follows.

Newton's law may be written

$$f = u_0 \frac{dm}{dt}$$

with $f = 100 \text{ lbf} = 4.4 \times 10^7 \text{ dyne}$. For the CM-RCS a typical firing time is about 100 milliseconds at a nominal flow rate of 0.357 lb/sec. The initial particle ejection velocity is then

$$u_0 = 4.4 \times 10^7 \text{ dynes} / 1.62 \times 10^3 \text{ gm/sec}$$

$$\therefore u_0 = 2.7 \times 10^4 \text{ cm/sec.}$$

Newkirk considers that the most important acceleration (or deceleration) mechanism is aerodynamic drag. This is certainly true for a nominal ATM orbit of 200 kilometers. For particles with a velocity component u with respect to the spacecraft, which is moving through a resisting medium of density ρ_a with velocity v , Newkirk considers the dynamic pressure to be

$$p_a \approx \rho_a (v + u)^2$$

where u is considered parallel to v . Since v is about 100 times greater than u , the acceleration of a particle of density ρ may be written

$$\dot{u} = \frac{3\rho_a v^2}{4\rho r}$$

Approximate values are

$$\rho_a \approx 1 \times 10^{-13} \text{ gm/cm}^3$$

and

$$v \approx 7.45 \times 10^7 \text{ cm/sec}$$

for a 200-kilometer-circular orbit. The specific density of exhaust material is approximately 1. For a particle of radius $r = 3\mu$

$$\dot{u} \approx 1.39 \times 10^2 \text{ cm/sec}^2.$$

For a particle of radius $r = 100\mu$,

$$\dot{u} \approx 4.17 \text{ cm/sec}^2.$$

The maximum time τ required for the drag force to stop an ejected particle is ≈ 50 seconds for a 3μ -particle and $\approx 6,400$ seconds for a 100μ -particle. These estimates differ from those given by Newkirk, since different firing times and mass flow rates are used here. Newkirk considers 200 grams exhausted every 20 minutes in arriving at estimates of lifetimes of 1,000 seconds and 40,000 seconds for 3μ and 100μ particles, respectively, released from the orientation jets of an Apollo spacecraft in a 320-kilometer orbit. The calculations made here are based on a shorter duration mass ejection period (in addition to somewhat different configurational assumptions) and provide shorter residence times for the ejected material.

It should be noted that this calculation illustrates only the residence time per particle, as defined by Newkirk and does not consider the amounts of material present.

REFERENCES

1. Piezih, E. T., "High-vacuum Plume Impingement Test Correlation," SID-64-1563, North American (August 1964)
2. Blackledge, M. L. and A. W. Lublowitz, "Investigation of LEM-RCS Thruster Plume Impingement on ATM Solar Panels," LMSC/HREC A784080, Contract NAS8-21003 (March 21, 1967)
3. North American Aviation, "SM and LEM Plume Impingement," MICL-05079-414 (June 1965)
4. Baker, L. R. and M. L. Blackledge, "Comparison of Real Gas and Perfect Gas Plume Flow Fields for the LEM Thruster Nozzle", LMSC/HREC TDR A781088 (March 1967)
5. Prozan, R. J., "Development of a Method-of-characteristics Solution for Supersonic Flow of an Ideal, Frozen or Equilibrium Reacting Gas Mixture," LMSC/HREC A782535 (April 1966)
6. Blackledge, M. L. and L. R. Baker, Jr., "Calculation of Thrust Degradation and Resulting Impingement Forces Resulting from LEM/RCS Thruster Plume," LMSC/HREC A784177, Contract NAS8-21003 (March 30, 1967)
7. Africane, A., "Engineering Method to Predict Saturn V Vehicle and Launch Complex Environments Due to Rocket Jet Impingement Test Report," SID-1520, North American (July 29, 1965)
8. French, E. P., "Effect of Rocket Exhausts on Infrared Planet Sensors," J. Spacecraft, Volume 3, pp. 849-853 (1966)
9. McPherson, D. G., "ATM Contamination Study," Final Report CR-61173 on Contract NASw-1386, Ball Brothers, Boulder, Colorado (May 25, 1967)
10. Latvala, E. K. and T. P. Anderson, "Studies of the Spreading of Rocket Exhaust Jets at High Altitudes," Ballistic Missiles and Space Technology, Volume II, Pergamon Press, pp. 77-91 (1961).
11. Love, E. S. et al, "Experimental and Theoretical Studies of Axisymmetric Free Jets," NASA TR R-6, (1959).

12. Letyala, E. K., "Spreading of Rocket Exhaust Jets at High Altitudes," AEDC-TR-59-11, ASTIA AD-215866, Contract No. AF40(690)-700 S/A 13(59-1) AEDC (June 1959)
13. Luce, R. W. and P. O. Jarvinen, "An Approximate Method for Predicting Plume Sizes for Nozzle Flow into Still Air," AIAA J. Volume 6, pp. 182-183 (1968)
14. Hill, J. A. F. and R. H. Habert, "Gas Dynamics of High-altitude Rocket Plumes," MITRAS, Inc., Cambridge, Massachusetts, Report MC 61-18-R1 (1963)
15. Hill, J. A. F. and J. S. Deaver, "Analytical Approximation for the Flow from a Nozzle into a Vacuum," J. Spacecraft Volume 3, pp. 1552-1554 (1966)
16. Newkirk, G. J., "Optical Environment of Manned Spacecraft," Planet and Space Science, Volume 15, pp. 1267-1285 (1967)
17. Vick, A. R. et al, "Rocket Exhaust-Plume Problems and Some Recent Related Research", in The Fluid Dynamic Aspects of Space Flight, Vol. II, Gordon and Breach, New York (1966).
18. Sodek, B. A., "ATM Optical Contamination Study", Brown Engineering Company, Inc., Interim Report SSL-27579-1 (January 12, 1968)
19. Chou, C. Y. and B. A. Sodek, "ATM Optical Contamination Study: A Study of Rapidly Moving Body-Ionosphere Interactions and Their Effects on Contamination Particles", Brown Engineering Company, Inc., Interim Report RL-SSL-030 (April 1968)
20. Daugherty, R. L. Fluid Mechanical with Engineering Applications, McGraw-Hill, New York (1954)
21. Anon. "ATM System Handbook (Preliminary)", Lockheed Missile and Space Company, Sunnyvale, California, LMSC-A842246, (June 15, 1967)

